Climate change and high exposure increased costs and disruption to lives and livelihoods from flooding associated with exceptionally heavy rainfall in Central Europe

Authors

Joyce Kimutai, *Grantham Institute - Climate Change and the Environment, Imperial College, London, UK*
Robert Vautard, *Institut Pierre-Simon Laplace, Paris, France*
Mariam Zachariah, *Grantham Institute - Climate Change and the Environment, Imperial College London, UK*
Radim Tolasz, *Czech Hydrometeorological Institute, Ostrava, Czechia*
Veronika Šustková, *Czech Hydrometeorological Institute, Ostrava, Czechia*
Christophe Cassou, *LMD, Institut Pierre-Simon Laplace, Paris, France*
Petr Skalák, *Global Change Research Institute, České Budějovice, Czechia*
Ben Clarke, *Grantham Institute - Climate Change and the Environment, Imperial College London, UK*
Klaus Haslinger, *GeoSphere Austria, Vienna, Austria*
Maja Vahlberg, *Red Cross Red Crescent Climate Centre, The Hague, the Netherlands (based in Ubmeje/Umeå, Sweden)*
Roop Singh, *Red Cross Red Crescent Climate Centre, The Hague, The Netherlands (based in New Jersey, USA)*
Elisabeth Stephens, *Department of Meteorology, University of Reading, Reading, the UK; Red Cross Red Crescent Climate Centre, the Hague, the Netherlands*
Hannah Cloke, *Department of Meteorology & Geography and Environmental Science, University of Reading, Reading , the UK*
Emmanuel Raju, *Copenhagen Centre for Disaster Research, Global Health Section, University of Copenhagen, Copenhagen, Denmark*
Nick Baumgart, *Copenhagen Centre for Disaster Research, Global Health Section, University of Copenhagen, Copenhagen, Denmark*
Lisa Thalheimer, *United Nations University - Institute for Environment and Human Security, Bonn, Germany*
Bogdan Chojnicki, *Poznań University of Life Sciences · Department of Agrometeorology, Poland*
Friederike Otto, *Grantham Institute - Climate Change and the Environment, Imperial College, London, UK*

Review authors

Gerbrand Koren, *Copernicus Institute of Sustainable Development, Utrecht University, Utrecht, The Netherlands*
Sjoukje Philip, *Royal Netherlands Meteorological Institute (KNMI), De Bilt, The Netherlands*
Sarah Kew, *Royal Netherlands Meteorological Institute (KNMI), De Bilt, The Netherlands*
Paula Haro, *European Regional Office, International Federation of Red Cross and Red Crescent Societies (IFRC), Budapest, Hungary*
Jennifer Vibert, *European Regional Office, International Federation of Red Cross and Red Crescent Societies (IFRC), Budapest, Hungary*
Andreas von Weissenberg, *European Regional Office, International Federation of Red Cross and Red Crescent Societies (IFRC), Budapest, Hungary*

Main findings

- The intensity and duration of the heavy rainfall put immense pressure on civil protection. Emergency management systems across Europe had been reinforced after severe flooding over the last decades and largely worked well: despite the higher intensity and larger scale, the number of fatalities is lower than in earlier floods with 24 estimated at the time of writing, compared to e.g. 232 in 2002 when flooding affected Germany, Austria, Czechia, Romania, Slovakia, and Hungary and at least 100 in 1997 when only Germany, Poland and Czechia were hit by floods. They are also much lower than in the Western European floods in 2021 when over 200 people lost their lives.
- The heavy rainfall was caused by a Vb depression, which forms when cold polar air flows from the north over the Alps, meeting very warm air in Southern Europe. Vb depressions are rare, but usually associated with heavy rain over Central Europe. Analysing analogous weather systems in the observed record suggests that there is no robust change in the number of analogous Vb depressions since the 1950s.
- The frequency is not the only characteristic of Vb depressions that could potentially change in a warming climate, other drivers of rainfall can change and affect likelihood and intensity of the overall rainfall analysed in the remainder of this study. In today's climate, which is 1.3°C warmer than at the beginning of the industrial period, a rainfall event of this magnitude is a very rare event expected to occur about once every 100 to 300 years. As the event is by far the heaviest ever recorded, the exact return time is difficult to estimate based on only about 100 years of observed data. We use a 100 year return-time for the rest of analysis.
- To assess if human-induced climate change influenced the heavy rainfall, we first determine if there is a trend in the observations. When looking at the regional-scale described above, heavy four-day rainfall events have become about twice as likely and 20% more intense since the pre-industrial era. The estimates become more uncertain when looking at more local scales, and are limited in places in some of the observed data.
- To quantify the role of human-induced climate change on this increase, we analyse climate models that are able to simulate heavy rainfall in the area and combine these with the observation-based assessment. All models show an increase in intensity and likelihood as well, as expected from physical processes in a warming climate. The combined change, attributable to human-induced climate change, is roughly a doubling in likelihood and a 7% increase in intensity. The models are however not explicitly modelling convection, and new convection-permitting studies have shown that increases in precipitation may have been underestimated in lower-resolution climate models. Therefore, these results are conservative.
- Under a future warming scenario where the global temperature is 2°C higher than pre-industrial levels, climate models predict even heavier 4-day rainfall events, with a further expected increase of about 5% in rainfall intensity and a further 50% increase in likelihood compared to present day. Again, these numbers are probably too low, due to the underestimation of very heavy rainfall in available climate models.
- The areas affected by the floods, notably in sprawling urban centres along major rivers, had been identified as highly vulnerable to flooding. These regions include Nysa and Wroclaw in Poland, Bratislava in Slovakia, the eastern regions of Galati and Vaslu in România, lower Austria and Vienna, as well as Ostrava, Opava, Krnov, Jeseník and Litovel in Czechia. Infrastructure and emergency management systems built after lessons learned from previous floods have been severely tested and in many cases overwhelmed by the sheer magnitude and scale of these floods, leading to damages that are estimated to several billion Euros.

- These floods were well-forecast and the death toll is considerably lower compared to the 1997 and 2002 floods, pointing to the effectiveness of investments made in forecasting, early warning systems, and forecast-based action including evacuations, flood defences and pre-emptive water reservoir releases. However, any loss of life underscores the need for further enhancements to account for climate change in enacting flood defences at scale, and improving risk communication and emergency response plans.

1 Introduction

From the 12th to the 15th (and ongoing in some regions) of September 2024 a very large region in Central Europe, including Poland, Czechia, Austria, Romania, Hungary, Germany and Slovakia experienced very heavy rainfall, breaking local and national rainfall records over the period of four days. While the rain was extremely heavy in many locations, the exceptional extent of the event, stretching across many countries, covered a far larger area than previous devastating floods in 1997 and 2002 [Řezáčová et al., 2005]. The extreme rainfall led to flooding in all affected countries with severe consequences for lives and livelihoods. At least 24 people lost their lives (The Guardian, 2024; BNN, 2024) with several persons still missing several days after the event in Czechia (DW, 2024). All countries were affected by power cuts, leading to schools and factories closing as well as hospitals. In Austria and Poland several dams and in Czechia stable flood protection measures (dams around the Oder River in Ostrava) broke, causing severe and sudden flooding. Two bridges were washed away in Poland, and thousands of homes and public buildings damaged in Romania.

Almost two million people were affected by the flooding event (blue News, 2024). The most severe impacts in urban areas were in the Polish-Czech border region and Austria (The Guardian, 2024). Austria's state of Lower Austria declared itself a "catastrophe region", with many villages and towns, such as St. Pollen undercut or destroyed (The Guardian, 2024). According to the insurance institution Gallagher Re, the estimated insured losses in the region will range between 2 to 3 billion euros (Gallagher Re, 2024). In Nysa, Poland, 44,000 residents, including hospital patients, had to evacuate due to the risk of an embankment breach, and embankments required strengthening in Wroclaw, Poland where further impacts are anticipated later in the week as reservoirs are near capacity (BBC, 2024, Reuters, 2024, The Guardian, 2024, Tageschau, 2024). Poland declared a state of national calamity in the region of Lower Silesia and parts of the Opole and Silesia voivodeship. As of September 21, 2.39 million Polish residents in 749 towns were living under the special regime. In Czechia, extensive damage to infrastructure (bridges, roads, railways, public and private buildings, energy and telecommunications facilities) was recorded in the basin draining the Jeseníky Mountains (Opava, Opavice, Odra, Bělá, Desná) (Czech Radio). The third largest city Ostrava suffered a barrier breach, flooding industrial areas (BBC, 2024. The river Morava submerged over 70% of the city Litovel. (Reuters, 2024). In lower Austria and Vienna, 26 villages remained isolated and 1,750 people had to be evacuated to temporary shelters (Tageschau, 2024, IFRC, 2024). Across the region, roads, bridges, and infrastructure have been damaged, leaving 250,000 without power, and tens of thousands without access to water, and mobile networks (Red Cross Climate Centre, 2024, Reuters, 2024, BBC, 2024, BNN News, 2024). In Romania, mostly rural areas were hit, while reports from Moldova, Ukraine, and Slovenia are limited (DW, 2024). In Germany, cities like Dresden are preparing for impacts after the event studied here, but estimates at that time suggested impacts will be less severe than anticipated (Tageschau, 2024).

The flooding displaced several hundred people across Poland, Czechia, Austria, Slovakia, Romania and Moldova. The displacement estimates mainly refer to evacuations between 13 and 16 September. In the Lower Silesia (Opole and Voivodeship) region of Poland 3,362 evacuees were reported. By Sunday 15 September, more than 13,500 people had been evacuated in Czechia alone, including 6,000 in the Moravian-Silesian region. Preventive evacuations continued in the following days, mainly in central and southern Moravia and southern Bohemia. In the Lower Austria region, 3,960 and 116 evacuees in the Bratislava region of Slovakia were reported. An additional 269 evacuees were reported across Galați and additional 46 evacuees in Vaslui county in România. In southern Moldova, about 160 people were evacuated (IDMC, 2024).

The heavy rainfall event from the 13th to 15th of September was caused by a so-called Vb (pronounced 5b) depression (Messmer et al., 2015). These low pressure systems form when cold polar air flows from the north over the Alps, deviates southwards initiating a cyclonic system in the lee side of the Alps and Northern Italy, which then develops and travels toward Central/Eastern Europe. Exceptionally-cold air masses moved over the Mediterranean/Adriatic Seas a few days before the rainfall event and became recharged in humidity before moving inland. In addition, backward trajectories from the affected area show a proportion of air parcels coming from Black Sea region, on the eastern flank of the low pressure system. Over the Black Sea, the SST anomaly is large (+2°C to +5°C), acting as a powerful energy source for evaporation of additional moisture. Mid-tropospheric air masses reaching East Austria on 12 September, were found to be mostly coming from Mediterranean areas, while on 15 September, they mostly originated from the western part of the Black Sea (Figure 1). In each case, polar air was flowing underneath, in the lowest part of the troposphere.

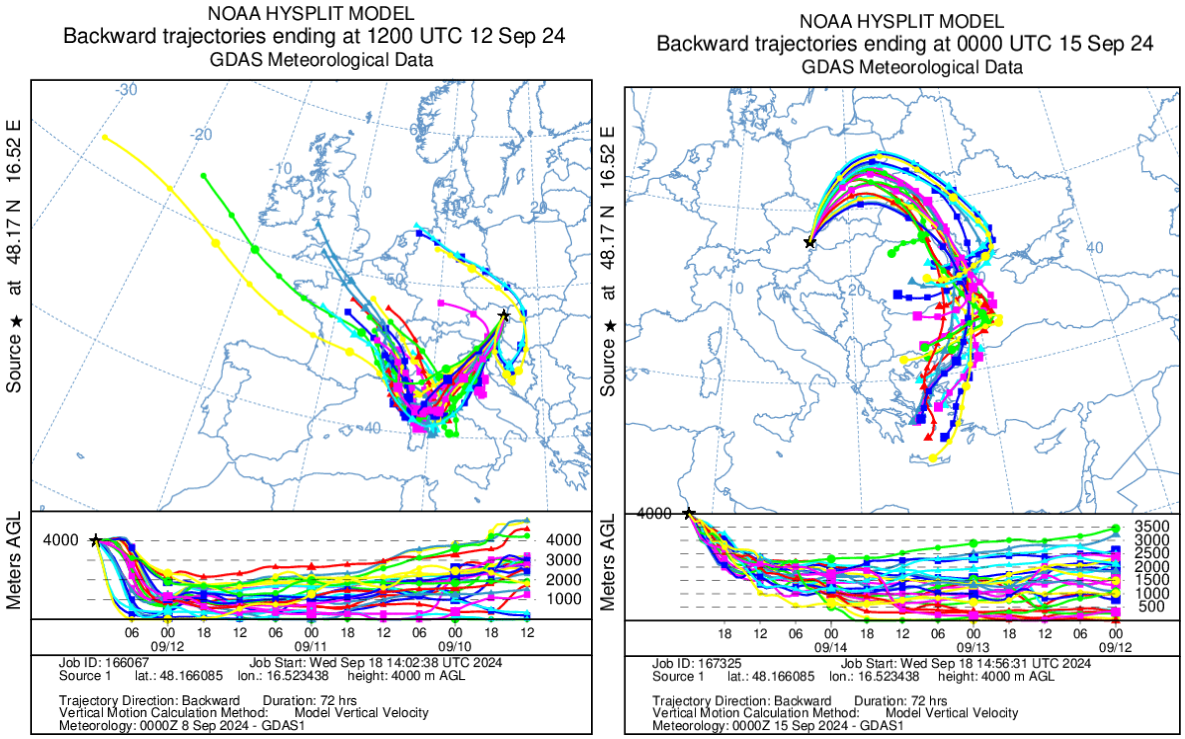

Figure1. 3-day backward trajectories for middle atmosphere (4000m, right) for Sept. the 12th (left) and Sept. the 15th (right). Lower panels show the evolution of the height of the parcel as a function of time

Figure 2 (top) shows the 500 hPa geopotential height over Europe on 14 September 2024, displaying a clear cut-off low centred over Central Europe, coupled with a strong anticyclone over Western Russia. This is associated with a south-easterly flow with warm air and moisture, in the middle troposphere, entrained from the western side of the Black Sea. The convergence of humidity forms a humid conveyer belt from Romania and Ukraine, to Poland, Czechia and Austria. Precipitable water reached rare levels (bottom) along the moisture path. Values were locally above the 99th percentile as calculated from the ERA5 reanalysis from 1979 to 2021 for this area, and were likely explained by the combined source of moisture from the Eastern Mediterranean basin and the Black Sea, both being extremely anomalously warm.

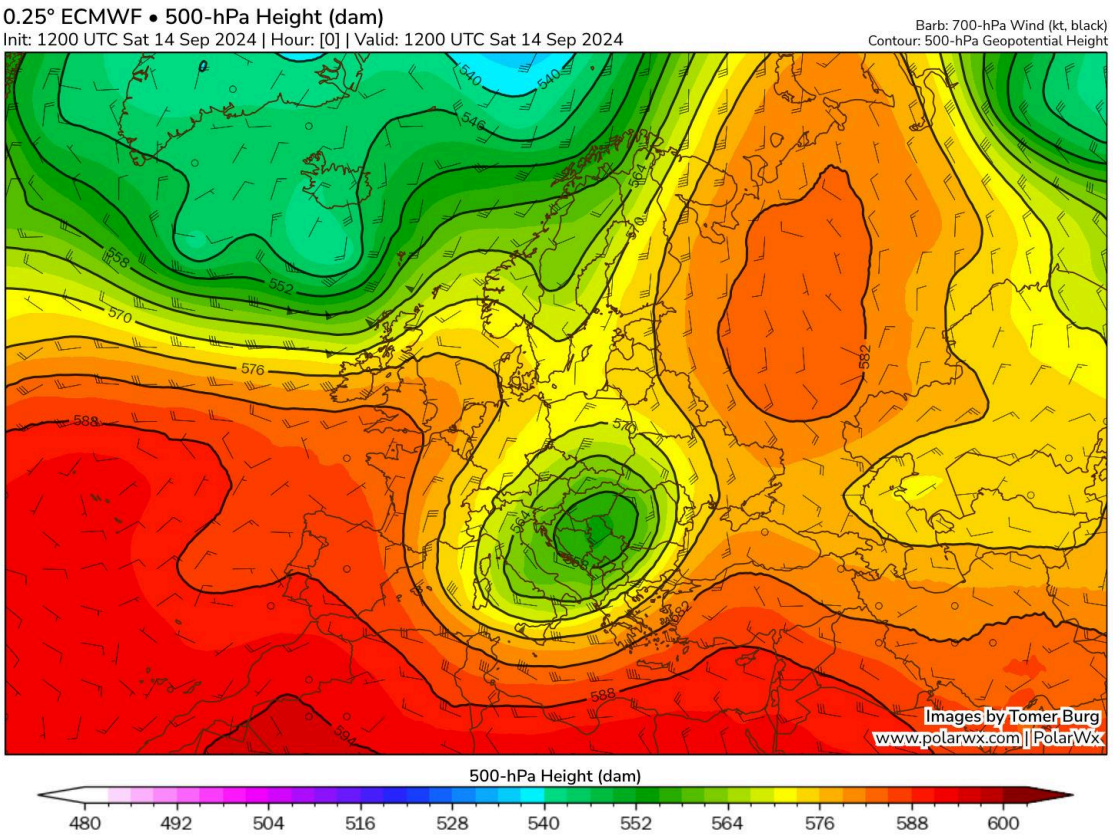

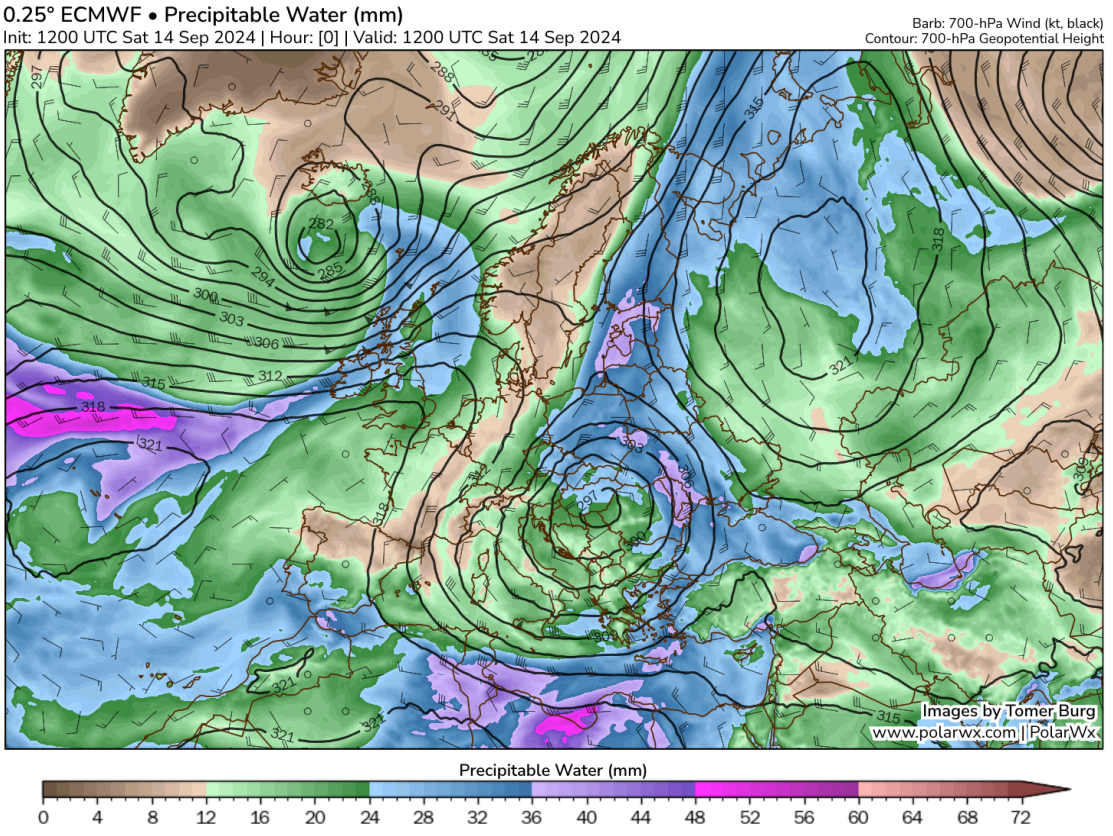

Figure 2: ECMWF analysis (ERA5T) on Saturday the 14th of September 2024, at 12:00, for (top) 500 hPa geopotential height (colour and lines) together with 700hPa wind (vectors), (bottom) for precipitable water

column (mm, colours) and 700hPa geopotential height (contours). Image built from the PolarWx web-interface)

1.1 Trend analysis of 500-hPa geopotential height anomalies

Vb weather conditions are comparatively rare, but usually bring large amounts of precipitation. One question is whether one sees a trend of more or less Vb cases with climate change. This question cannot be addressed in detail in this rapid study as it would require applying a detection method (eg. tracking) for these events. However, we addressed a simpler question, whether one detects a trend in the frequency of analogues of the mean anomaly found in the 500 hPa geopotential height over the four days from 12 Sep to 15 Sep, associated with the cut-off low, as for the 14 Sep in Figure 3. For each June-September period of each year between 1950 and 2024, we selected days when the 500 hPa anomaly correlation with the geopotential field of the focus period exceeds a threshold correlation ('Co': 0.6 to 0.8). For Co=0.8, generally less than 10 analogue periods were found each year, and no significant trend could be found. This would indicate that such cut-off low in terms of spatial structure does not have an increasing or decreasing frequency. However, ClimaMeter suggested a deepening of similar pressure systems as Boris, mainly at its central point for the 2024 event, using analogue techniques, up to 200 hPa, with potential consequences of increasing rainfall. This could imply that the trends in such pressure systems could be sensitive to the method used.

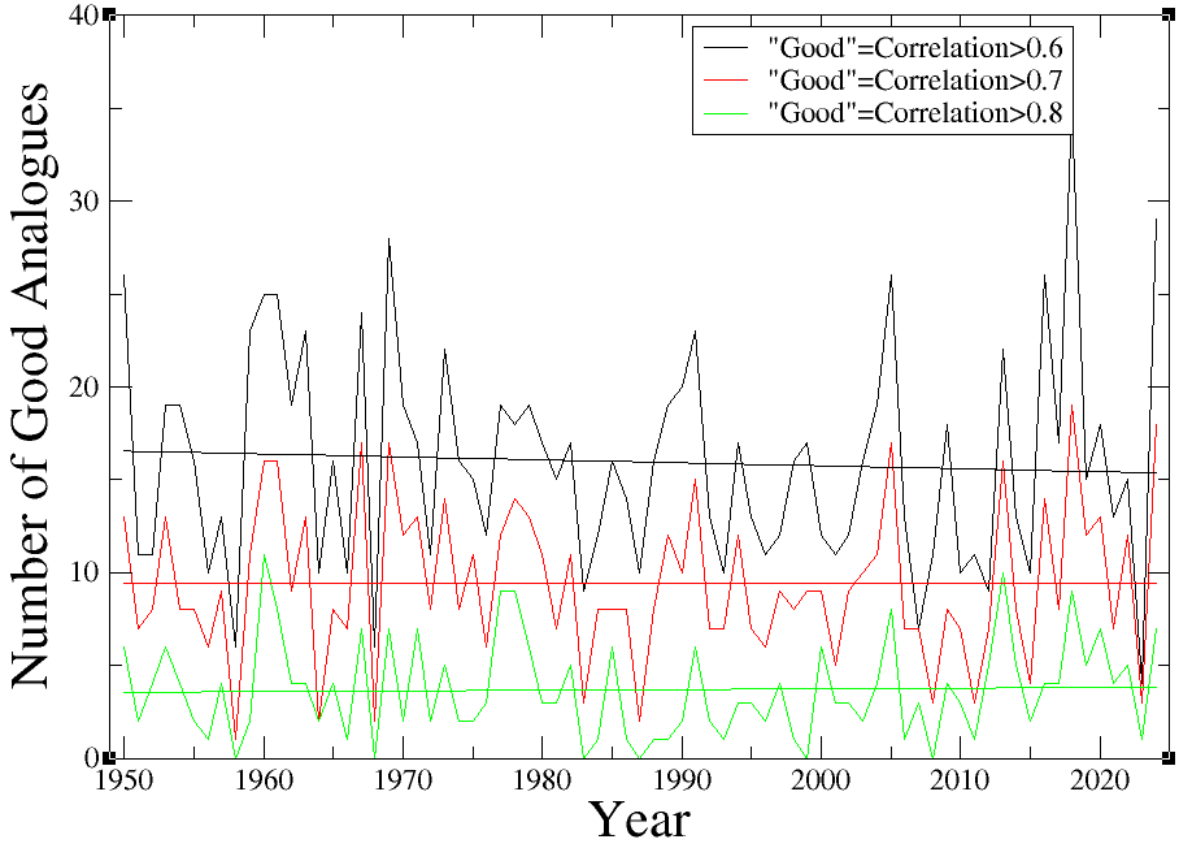

Figure 3. Number of "good" analogues per year (in the June-September period) of the mean 500 hPa geopotential height over the 12-15 September 2024. "Good analogues" are found when the anomaly correlation between the two 4-day averages is above a threshold, in this figure 0.6, 0.7 or 0.8. The anomaly correlation is calculated over a region encompassing the cut-off low [-10° to 40°E; 30° to 60°N]

Although rather rare, Vb events are responsible for 45% of extreme precipitation events in northern Austria (Hofstätter et al. 2017), the area most affected by the current event. The 50 strongest Vb events during recent decades show increases in precipitation of 7-20% north of the Alpine ridge (Hofstätter et al. 2017). The current event 5-day rainfall sums exceeded 350mm in vast areas of the federal state of Lower Austria, at some places showing two-fold increases of 5-day rainfall sums compared to the former top ranked event (GeoSphere Austria). As in Austria, the synoptic Vb situation is not very frequent in Czechia, but it is usually the cause of high rainfall in larger areas of the country. In this context, it is worth recalling the extraordinary floods in June 1997 in Moravia and in August 2002 in Bohemia. In September 2024, the highest five-day rainfall totals were recorded in Moravia (Bělá pod Pradědem 546 mm, Jeseník 536 mm, Zlaté hory 492 mm, Paprsek 480 mm, Slaměnka 471 mm, Dlouhé Stráně 450 mm), but also in Bohemia (Labská bouda 528 mm, Pomezní boudy 518 mm, Luční bouda 456 mm). A total of 130 out of 450 basic precipitation measuring stations in Czechia recorded a five-day total of more than 200 mm.

1.2 Event Definition

The impacted areas were affected by heavy downpour that lasted from 12 to 15th Sep. We chose the wettest 4-day period in the year, the annual 4-day maximum accumulated rainfall over the study region (red box in Figure 4). While the event is still ongoing in some regions, this timeframe represents the wettest continuous period during the event up to the time of writing. The decision to analyse this specific region and temporal period was based on availability of data and the importance to capture the most significant impacts within the event's early stages. We selected a broad region, spanning multiple countries (Poland, Czechia, Austria, Romania, Hungary, Germany and Slovakia) that experienced record-breaking rainfall and widespread flooding and was severely affected. For both ERA5 and MSWEP datasets, the flood-inducing event was exceptional in the region (Figure 5). The RX4day metric allows us to quantify the intensity of the event within the most critical period. However, we recognize that more in-depth studies are necessary to fully understand other aspects of the event, including interaction of dynamics and thermodynamics. Refining the spatial and temporal definition could provide more localised insights into return periods, trends, and the specific impacts of climate change on these regions. Therefore potential future studies can be used to analyse other aspects of this flooding event. In this report, we study the influence of anthropogenic climate change by comparing the likelihood and intensity of similar RX4day events at present with those in a 1.3 °C cooler climate. We also extend this analysis into the future by assessing the influence of a further 0.7 °C of global warming from present.

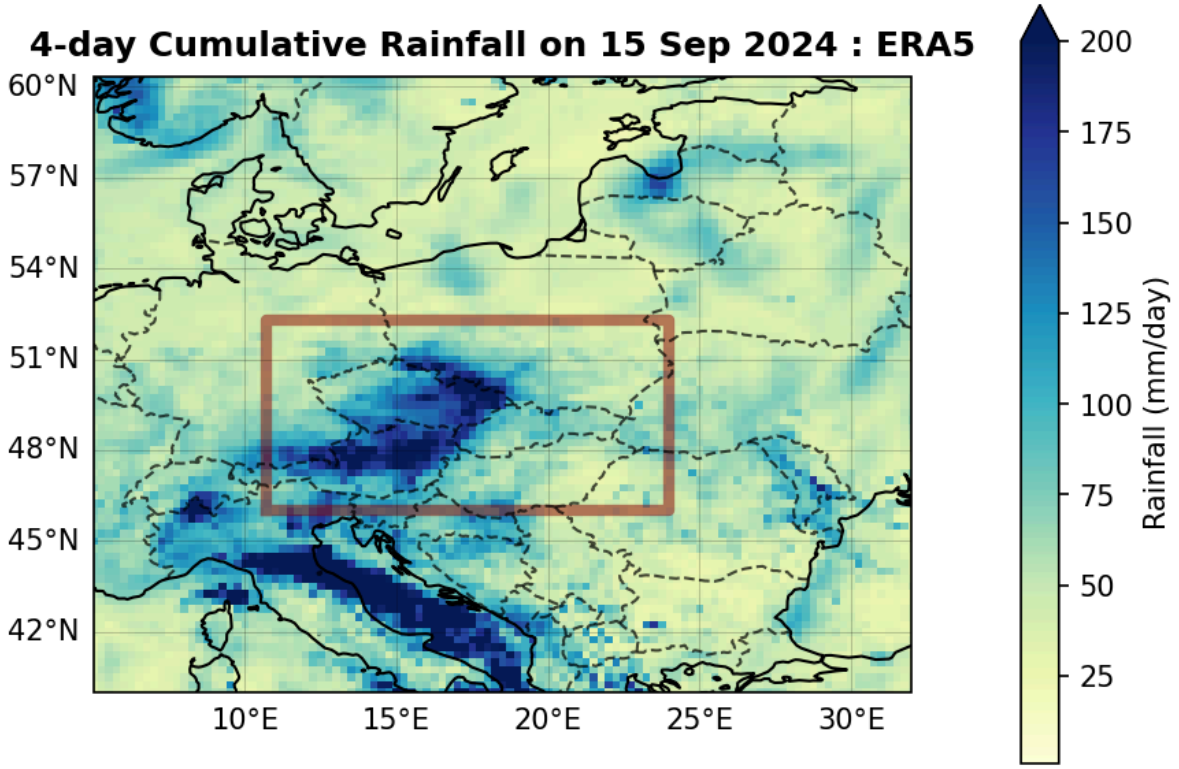

Figure 4. Map of accumulated precipitation during the wettest annual 4-day period over the study region (outlined in red) during September 2024, based on ERA5 dataset.

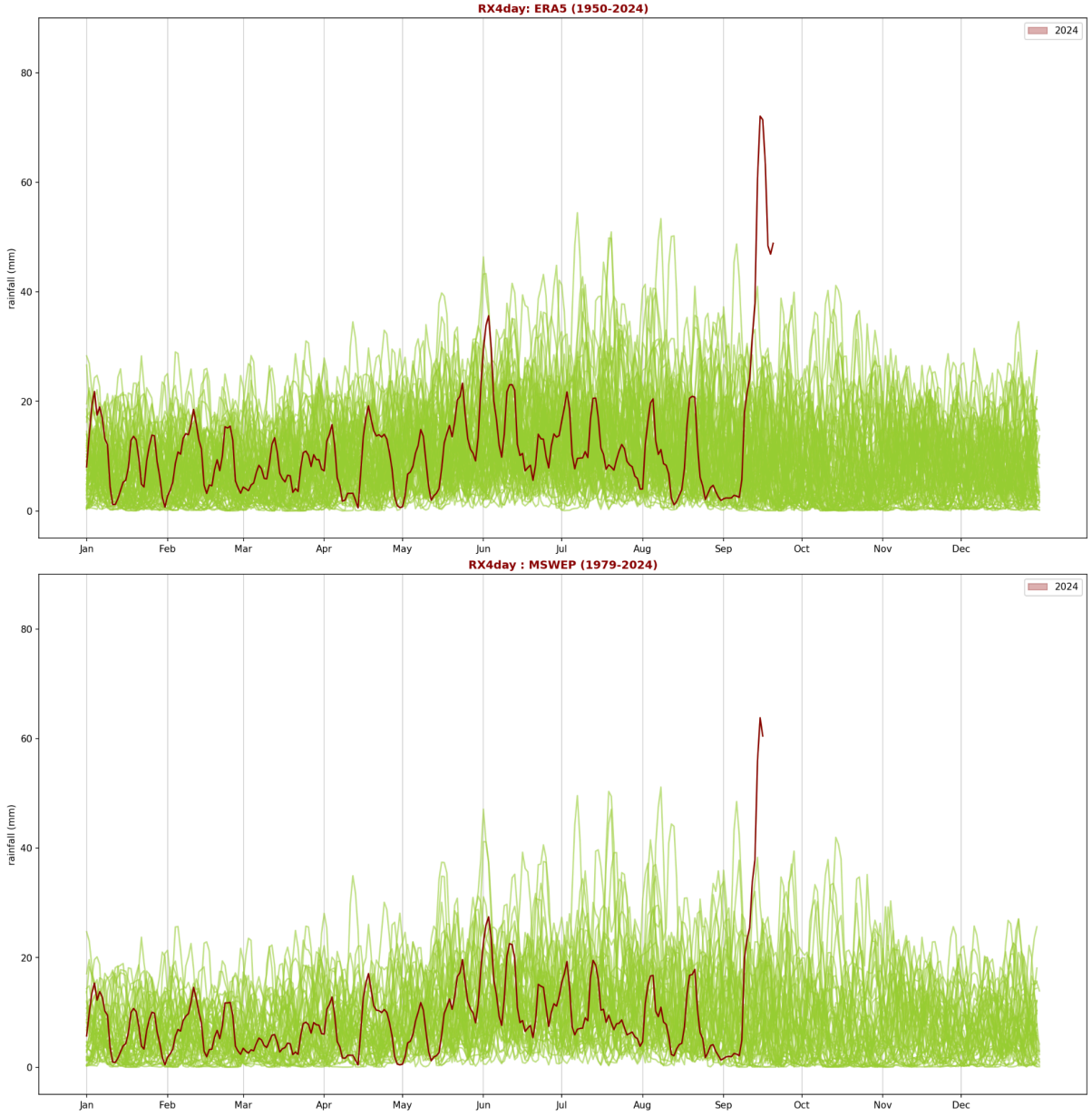

Figure 5. 4-day cumulative rainfall over the study region from 1950-2024 based on ERA5 (top) and from 1979-2024 based on MSWEP (bottom). The brown line shows RX4day in 2024 with exceptional levels in September 2024.

2 Data and methods

2.1 Observational data

In this study, we utilised three gridded datasets and station data from Czechia and Austria, as described below.

2.1.1 Gridded datasets

In this study, we utilise three gridded datasets.

- **ERA5**.The European Centre for Medium-Range Weather Forecasts's 5th generation reanalysis product, ERA5, is a gridded dataset that combines historical observations into global estimates using advanced modelling and data assimilation systems (Hersbach et al., 2020). We use daily precipitation data spanning 1950-2024 data from this product at a resolution of 0.25° x 0.25°. The re-analysis is available until the 31st of August 2024. We extend the re-analysis data with the ECMWF analysis and forecasts till the 15 Sep.
- **MSWEP**. The Multi-Source Weighted-Ensemble Precipitation (MSWEP) v2.8 dataset (updated from Beck et al., 2019) is fully global, available at 3-hourly intervals and at 0.1° spatial resolution, available from 1979 to ~3 hours from real-time. This product combines gauge-, satellite-, and reanalysis-based data. In this dataset, we utilise daily rainfall data from 1979-Sep 2024.
- **E-OBS.** E-OBS (version 28.0e), is a 0.25° × 0.25° gridded temperature dataset of Europe, formed from the interpolation of station-derived meteorological observations (Cornes et al., 2018). As data for the event (September 12–15) was not yet available, E-OBS was utilised to assess and complement the analysis of trends in RX4day for the region using return periods obtained from ERA5 and MSWEP.

2.1.2 Station data

We use daily observed rainfall data from two stations in Czechia (provided by the Czech Hydrometeorological Institute) and four stations in Austria (provided by Geosphere Austria). The data varies in length, with most records dating back to 1950. For these stations, we assess trends and compare them with gridded datasets for the event period.

2.1.3 Global Mean Surface Temperature (GMST)

As a measure of anthropogenic climate change we use the (low-pass filtered) global mean surface temperature (GMST), where GMST is taken from the National Aeronautics and Space Administration (NASA) Goddard Institute for Space Science (GISS) surface temperature analysis (GISTEMP, Hansen et al., 2010 and Lenssen et al. 2019).

2.2 Model and experiment descriptions

We use two multi-model ensembles from climate modelling experiments using very different framings (Philip et al., 2020): Sea Surface temperature (SST) driven global circulation high resolution models, coupled global circulation models and regional climate models.

1. **CORDEX** Coordinated Regional Climate Downscaling Experiment (CORDEX)- European Domain (EURO-CORDEX) with 0.11° resolution (EUR-11) (Jacob et al., 2014; Vautard et al., 2021). The ensemble used in this study consists of 9 regional climate models which are

driven by one or more of 6 GCMs. These simulations are composed of historical simulations up to 2005, and extended to the year 2100 using the RCP8.5 scenario.

2. **CMIP6** Couple Model Intercomparison Project phase 6- This study uses simulations from 13 models with varying resolutions. For more details on CMIP6, please see Eyring et al., (2016). For all simulations, the period 1850 to 2015 is based on historical simulations, while the SSP5-8.5 scenario is used for the remainder of the 21st century.

2.3 Statistical methods

Methods for observational and model analysis, and for model evaluation and synthesis are used according to the World Weather Attribution Protocol, described in Philip et al., (2020), with supporting details found in van Oldenborgh et al., (2021), Ciavarella et al., (2021) and here. The key steps, presented in sections 3-6, are: (3) trend estimation from observations; (4) model validation; (5) multi-method multi-model attribution; and (6) synthesis of the attribution statement. In this report, we analyse the time series of annual maximum accumulated 4-day rainfall (RX4day), area-averaged over the study region described in Section 1.2, extracted from the three observed gridded datasets described in Section 2.1.1 and the climate models described in Section 2.2. A non-stationary Generalised Extreme Value (GEV) distribution is used to model RX4day. The distribution is assumed to scale exponentially with the covariates, with the dispersion (the ratio between the standard deviation and the mean) remaining constant over time. The parameters of the statistical model are estimated using maximum likelihood. For each time series, we calculate the return periods, probability ratio (PR; the factor-change in the event's probability) and change in intensity of the event under study for the 2024 GMST and for 1.3 C cooler GMST: this allows us to compare the climate of now and of the preindustrial past (1850-1900, based on the Global Warming Index).
The variable of interest , X, is assumed to follow a GEV distribution in which the location and scale parameters vary with GMST:

$$X \sim GEV(\mu, \sigma, \xi \mid \mu_0, \sigma_0, \alpha, T),$$

where X denotes the variable of interest- RX4day in this case; T is the smoothed GMST; μ_0, σ_0 and ξ are the location, scale and shape parameters of the nonstationary distribution; and α is the trend due to GMST. As a result, the location and scale of the distribution have a different value in each year, determined by the GMST state of that year. Maximum likelihood estimation is used to estimate the model parameters, with

$$\mu = \mu_0 exp\left(\frac{\alpha T}{\mu_o}\right) \qquad \text{and} \qquad \sigma = \sigma_0 exp\left(\frac{\alpha T}{\mu_o}\right).$$

This formulation reflects the Clausius-Clapeyron relation, which implies that precipitation scales exponentially with temperature (Trenberth et.al., 2003, O'Gorman and Schneider 2009).

3 Observational analysis: return period and trend

3.1 Analysis of gridded data and point station data

We assess trends in RX4day over the region encompassing Poland, Czechia, Austria, Romania, Hungary, Germany and Slovakia. To enhance the analysis, for observations, we also examined trends within subregions, individual countries, and specific stations located in the study area. Figure 3.1 shows these trends as observed in ERA5, MSWEP, and E-OBS. For E-OBS, we used return periods from ERA5 and MSWEP due to the lack of data extending to 2024. All datasets show similar trends across the region, with increasing trends, though the increases are less pronounced in MSWEP and E-OBS.

In Table 3.1, we present the estimated return periods and changes in both the probability and magnitude of the event across the study region using three datasets. The return period for the 2024 event is estimated at 201 years (uncertainty: 25 years to infinity) in ERA5, 100 years (25 to 7429 years) in E-OBS, and 97 years (20 years to infinity) in MSWEP. The best estimates for the probability ratio between the 2024 climate and a climate 1.3°C cooler show an increase across all datasets, although this increase is not statistically significant in E-OBS and MSWEP. The intensity estimates indicate an 18% increase in ERA5, a 51% increase in E-OBS, and a 1.3% decrease in MSWEP. The increase in E-OBS is statistically significant, while the change in ERA5 centres on no change, and the decrease in MSWEP is not statistically significant. A return period of 100 years is used to assess RX4day changes in climate models.

Table 3.2 presents the estimated return periods and changes in both the probability and magnitude of the event across Czechia, Hungary, Slovakia, Austria, and four sub-regions (divided into approximate quadrants along the lines 17 °E and 48 °N) using ERA5 data only. For all countries and subregions, we observe an increase in the probability ratio and event magnitude, though not statistically significant in all cases. Statistically significant changes are found in Czechia (PR 3.53 [1.60 - 34.17], magnitude change 31.28% [10.16 - 59.14]) and Hungary (PR 4.67 [1.47 - 36.26], magnitude change 23.30% [4.30 - 50.12]). In Slovakia (PR 5.18 [0.49 - inf], magnitude change 16.09% [-6.29 - 47.67]) and Hungary (PR 2.24 [0.72 - 12.15], magnitude change 13.60% [-2.62 - 35.42]), the changes are not statistically significant. Among the subregions, statistically significant increases in both event magnitude and likelihood are observed in both western quadrants. Statistical fits to the subregions are shown in the appendix.

For the station data, the GEV scale fit does not apply well to some stations, as the variance increases significantly while the mean decreases slightly (Figs. S4-S5). Probability ratios and intensity changes between the current climate and a 1.3degC cooler world for these stations are listed in Table 3.3. We observe increasing rainfall magnitudes in Langlenbarn and St.Pölten, but decreases in the other stations. However, when applying the scale+shift assumption, trends increase in Weyer, Zlate Hory, Jesenik, and Langlenbarn, but decrease in St.Pölten. We therefore conclude we cannot draw a robust conclusion on trends from station data.

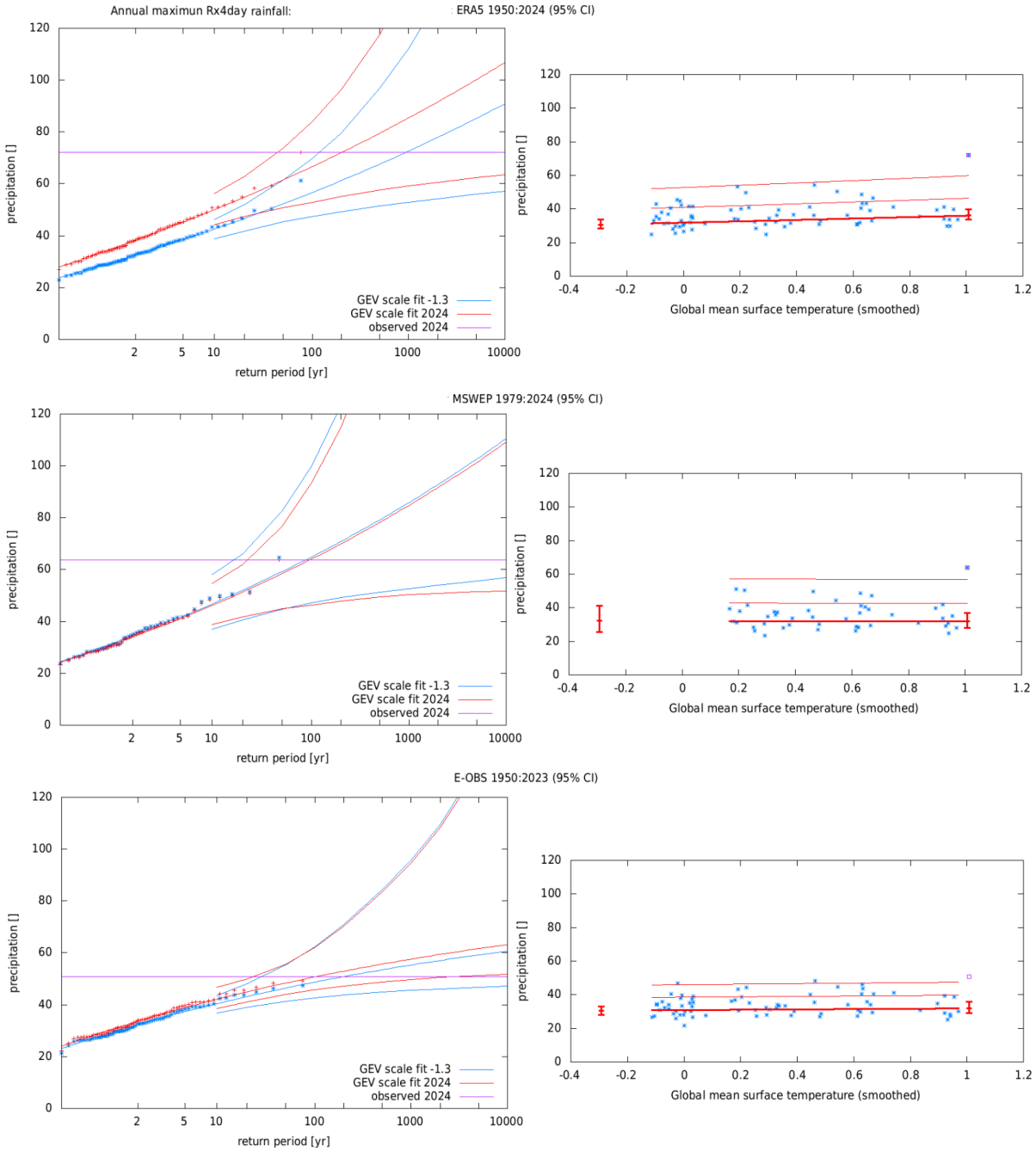

Figure 6. Response of RX4day to change in GMST, based on the ERA5 (top) and MSWEP (centre) and E-OBS (bottom) datasets. Left: Changes in return periods based on 2024 GMST (red lines) and 1.3°C lower GMST (blue lines). Right: Trends in RX4day. The thick red line denotes the time-varying mean, and the thin red lines show 1 standard deviation (s.d) and 2 s.d above. The vertical red lines show the 95% confidence interval for the location parameter, for the current, 2024 climate and the hypothetical, 1.2ºC cooler climate. The 2024 event is highlighted with the magenta box.

Table 3.1: Change in probability ratio and magnitude for Annual RX4day in the study region due to GMST. Light blue indicates an increasing trend that encompasses no change, while dark blue indicates a statistically significant increasing trend. Light orange indicates a decreasing trend, while dark orange indicates a statistically significant decreasing trend.

	Event	**GMST (Covariate)**

Dataset	Magnitude (mm)	Return period (95% C.I.)	Probability Ratio	Change in magnitude (%)
ERA5	72.1	201 (46 … inf)	4.6 (1.2 ... 5.4e+4)	18 (0.64 ... 36)
E-OBS	50.7	100 (24 …7429)	1.9 (0.20 ... 1.6e+3)	51 (45 ... 62)
MSWEP	63.8	97 (20.25 … inf)	1.1 (0.0 ... 5.7e+2)	-1.3 (-28 ... 36)

Table 3.2: Change in probability ratio and magnitude for annual RX4day in the subregions/countries within the study region due to GMST. Light blue indicates an increasing trend that encompasses no change, while dark blue indicates a statistically significant increasing trend. Light orange indicates a decreasing trend, while dark orange indicates a statistically significant decreasing trend.

Subregion	Return period (95% C.I.)	Probability Ratio	Change in magnitude (%)
Czechia	156.7	3.53 (1.60 - 34.17)	31.28 (10.16 - 59.14)
Hungary	6.33	4.67 (1.47 - 36.26)	23.30 (4.30 - 50.12)
Slovakia	32.8	5.18 (0.49 - inf)	16.09 (-6.29 - 47.67)
Austria	163	2.24 (0.72 - 12.15)	13.60 (-2.62 - 35.42)
NW quadrant	130.7	3.28 (1.41 - 16.75)	25.47 (5.91 - 47.71)
NE quadrant	2.5	2.32 (0.76 - 15.75)	14.55 (-4.39 - 39.55)
SW quadrant	136.6	3.19 (1.43 - 9.24)	22.36 (7.13 - 37.90)
SE quadrant	1.58	1.94 (0.72 - 6.51)	11.05 (-5.20 - 34.0)

Table 3.3: Probability ratio and change in magnitude between the 2024 climate and 1.3degC cooler climate for annual RX4day in stations within the study region due to GMST. Light blue indicates an increasing trend that encompasses no change, while dark blue indicates a statistically significant increasing trend. Light orange indicates a decreasing trend, while dark orange indicates a statistically significant decreasing trend.

Station	Probability Ratio	Change in magnitude (%)
Jesenik	0.35(0.85E-03 ... 2.26)	-23.57(-54.15 ... 38.38)
Zlate hory	0.65(0.51E-01 ... 4.3639)	-11.12(-48.02 ... 49.5)
Langlenbarn	2.37(0.38 ... 88.0)	23.72(-17.101 ... 79.7)
St.Pölten	3.50(0.28086E-01 ... ∞)	17.47(-20.21 ... 75.01)
Weyer	0.87(0.48 ... 3.94)	-5.07(-21.63 ... 43.79)

4 Model evaluation

In the subsections below we show the results of the model evaluation for each location. For each framing or model setup we also use models that only just pass the evaluation tests if we only have five models or less for that framing that perform well. Table 4.1 shows the model evaluation results. In this section we show the results of the model evaluation for the assessed region. The climate models are evaluated against the observations in their ability to capture:

1. Seasonal cycles: For this, we qualitatively compare the seasonal cycles based on model outputs against observations-based cycles. We discard the models that exhibit ill-defined peaks in their seasonal cycles. We also discard the model if the rainy season onset/termination varies significantly from the observations.

2. Spatial patterns: Models that do not match the observations in terms of the large-scale precipitation patterns are excluded.

3. Parameters of the fitted statistical models. We discard the model if the model and observation parameters ranges do not overlap.

The models are labelled as 'good','reasonable', or 'bad' based on their performances in terms of the three criteria discussed above. A model is given an overall rating of 'good' if it is rated 'good' for all three characteristics. If there is at least one 'reasonable', then its overall rating will be 'reasonable' and 'bad' if there is at least one 'bad'.

Table 4.1 Evaluation results of the climate models considered for attribution analysis of Rx4day. For each model, the threshold for a 1-in-100-year event is shown, along with the best estimates of the Dispersion and Shape parameters are shown, along with the 95% confidence intervals. Furthermore evaluation results of the seasonal cycle and spatial pattern are shown.

Model / Observations	**Seasonal cycle**	**Spatial pattern**	**Dispersion**	**Shape parameter**	**Overall rating**
ERA5 (1950)			0.160 (0.129 ... 0.185)	0.059 (-0.14 ... 0.24)	
E-OBS (1950)			0.157 (0.115 ... 0.183)	-0.92 (0.021 ... inf)	
MSWEP (1979)			0.186 (0.138 ... 0.228)	0.072 (-0.28 ... 0.41)	
CMIP6					
CMCC-CM2-SR5 (1)	good	bad	0.154 (0.0961 ... 0.201)	0.054 (-0.34 ... 0.62)	bad
CMCC-ESM2 (1)	bad	bad	0.165 (0.106 ... 0.211)	-0.14 (-0.60 ... 0.43)	bad
E3SM-1-0 (1)	good	good	0.125 (0.0847 ... 0.153)	-0.18 (-0.73 ... 0.24)	good
EC-Earth3-CC (1)	good	good	0.140 (0.0889 ... 0.172)	-0.095 (-0.61 ... 0.50)	good

EC-Earth3-Veg (1)	reasonable	good	0.171 (0.0814 ... 0.217)	-0.0036 (-0.38 ... 1.0)	reasonable
EC-Earth3-Veg-LR (1)	good	good	0.154 (0.102 ... 0.187)	0.080 (-0.40 ... 0.68)	good
INM-CM4-8 (1)	bad	reasonable	0.167 (0.0816 ... 0.213)	-0.062 (-0.42 ... 0.70)	bad
INM-CM5-0 (1)	bad	reasonable	0.146 (0.100 ... 0.180)	0.017 (-0.56 ... 0.49)	bad
IPSL-CM6A-LR (1)	reasonable	good	0.155 (0.0972 ... 0.201)	0.10 (-0.40 ... 0.69)	reasonable
KACE-1-0-G (1)	bad	good	0.154 (0.111 ... 0.182)	-0.27 (-0.76 ... 0.12)	bad
MPI-ESM1-2-HR (1)	reasonable	reasonable	0.204 (0.141 ... 0.252)	-0.014 (-0.44 ... 0.44)	reasonable
MPI-ESM1-2-LR (1)	reasonable	reasonable	0.156 (0.112 ... 0.191)	0.0069 (-0.31 ... 0.34)	reasonable
NESM3 (1)	reasonable	reasonable	0.186 (0.111 ... 0.223)	-0.38 (-0.76 ... 0.31)	reasonable
CORDEX					
CNRM-CM5_rcp85_r1i1p1_CCLM4-8-17 (1)	bad	good			bad
CNRM-CM5_rcp85_r1i1p1_ETH-COSMO-crCLIM-v1-1 (1)	reasonable	good	0.146 (0.105 ... 0.196)	-0.066 (-0.57 ... 0.26)	reasonable
CNRM-CM5_rcp85_r1i1p1_RACMO22E (1)	reasonable	reasonable	0.0965 (0.0599 ... 0.120)	-0.22 (-0.58 ... 0.20)	reasonable
CNRM-CM5_rcp85_r1i1p1_RegCM4-6 (1)	reasonable	reasonable	0.161 (0.107 ... 0.196)	-0.089 (-0.43 ... 0.34)	reasonable
CNRM-CM5_rcp85_r1i1p1_REMO2015 (1)	reasonable	reasonable	0.150 (0.103 ... 0.182)	-0.083 (-0.41 ... 0.28)	reasonable
CNRM-CM5_rcp85_r1i1p1_UGent-ALARO-0 (1)	reasonable	reasonable	0.124 (0.0801 ... 0.146)	-0.14 (-0.44 ... 0.42)	reasonable
EC-EARTH_rcp85_r12i1p1_CCLM4-8-17 (1)	reasonable	good	0.166 (0.0977 ... 0.198)	0.059 (-0.29 ... 0.72)	reasonable
EC-EARTH_rcp85_r12i1p1_ETH-COSMO-crCLIM-v1-1 (1)	reasonable	good	0.171 (0.123 ... 0.205)	0.020 (-0.47 ... 0.42)	reasonable
EC-EARTH_rcp85_r12i1p1_RACMO22E (1)	good	reasonable	0.183 (0.133 ... 0.225)	-0.38 (-0.84 ... -0.099)	reasonable
EC-EARTH_rcp85_r12i1p1_RegCM4-6 (1)	reasonable	reasonable	0.166 (0.117 ... 0.209)	-0.020 (-0.37 ... 0.33)	reasonable
EC-EARTH_rcp85_r1i1p1_ETH-COSMO-crCLIM-v1-1 (1)	reasonable	good	0.185 (0.125 ... 0.259)	0.10 (-0.55 ... 0.64)	reasonable

EC-EARTH_rcp85_r1i1p1_RACMO22E (1)	good	reasonable	0.194 (0.139 ... 0.238)	-0.60 (-0.89 ... -0.11)	reasonable
EC-EARTH_rcp85_r3i1p1_ETH-COSMO-crCLIM-v1-1 (1)	reasonable	good	0.142 (0.0755 ... 0.184)	-0.034 (-0.46 ... 1.0)	reasonable
EC-EARTH_rcp85_r3i1p1_RACMO22E (1)	good	reasonable	0.165 (0.107 ... 0.203)	-0.091 (-0.42 ... 0.39)	reasonable
HadGEM2-ES_rcp85_r1i1p1_CCLM4-8-17 (1)	bad	good	0.129 (0.0846 ... 0.163)	-0.17 (-0.57 ... 0.29)	bad
HadGEM2-ES_rcp85_r1i1p1_ETH-COSMO-crCLIM-v1-1 (1)	bad	reasonable	0.151 (0.104 ... 0.182)	-0.12 (-0.49 ... 0.35)	bad
HadGEM2-ES_rcp85_r1i1p1_RACMO22E (1)	reasonable	reasonable	0.138 (0.0861 ... 0.170)	0.019 (-0.31 ... 0.57)	reasonable
HadGEM2-ES_rcp85_r1i1p1_RegCM4-6 (1)	bad	reasonable	0.141 (0.0830 ... 0.172)	0.075 (-0.31 ... 0.65)	bad
IPSL-CM5A-MR_rcp85_r1i1p1_RACMO22E (1)	good	reasonable	0.143 (0.102 ... 0.178)	0.00048 (-0.31 ... 0.28)	reasonable
IPSL-CM5A-MR_rcp85_r1i1p1_REMO2015 (1)	reasonable	reasonable	0.169 (0.104 ... 0.210)	-0.13 (-0.55 ... 0.49)	reasonable
MPI-ESM-LR_rcp85_r1i1p1_CCLM4-8-17 (1)	good	good	0.120 (0.0767 ... 0.148)	0.11 (-0.30 ... 0.54)	good
MPI-ESM-LR_rcp85_r1i1p1_CSC-REMO2009 (1)	good	reasonable	0.133 (0.0866 ... 0.161)	-0.078 (-0.36 ... 0.30)	reasonable
MPI-ESM-LR_rcp85_r1i1p1_ETH-COSMO-crCLIM-v1-1 (1)	good	good	0.146 (0.0968 ... 0.185)	0.085 (-0.42 ... 0.59)	good
MPI-ESM-LR_rcp85_r1i1p1_RACMO22E (1)	good	reasonable	0.134 (0.0962 ... 0.164)	-0.30 (-0.77 ... 0.11)	reasonable
MPI-ESM-LR_rcp85_r1i1p1_RegCM4-6 (1)	reasonable	reasonable	0.153 (0.0910 ... 0.187)	-0.064 (-0.49 ... 0.32)	reasonable
MPI-ESM-LR_rcp85_r1i1p1_WRF361H (1)	good	reasonable	0.156 (0.0281 ... 0.230)	0.32 (-0.35 ... 3.8)	reasonable
MPI-ESM-LR_rcp85_r2i1p1_CSC-REMO2009 (1)	good	reasonable	0.148 (0.0833 ... 0.185)	-0.026 (-0.35 ... 0.45)	reasonable
MPI-ESM-LR_rcp85_r2i1p1_ETH-COSMO-crCLIM-v1-1 (1)	good	good	0.192 (0.143 ... 0.226)	-0.064 (-0.68 ... 0.25)	good
MPI-ESM-LR_rcp85_r3i1p1_ETH-COSMO-crCLIM-v1-1 (1)	good	good	0.0993 (0.0676 ... 0.125)	0.28 (-0.016 ... 0.76)	reasonable

MPI-ESM-LR_rcp85_r3i1p1_REMO2015 (1)	reasonable	reasonable	0.134 (0.0752 ... 0.161)	-0.010 (-0.40 ... 0.51)	reasonable
NorESM1-M_rcp85_r1i1p1_ETH-COSMO-crCLIM-v1-1 (1)	good	good	0.109 (0.0676 ... 0.133)	-0.27 (-0.57 ... 0.050)	reasonable
NorESM1-M_rcp85_r1i1p1_RACMO22E (1)	reasonable	reasonable	0.119 (0.0718 ... 0.152)	0.043 (-0.43 ... 0.77)	reasonable
NorESM1-M_rcp85_r1i1p1_RegCM4-6 (1)	bad	reasonable	0.185 (0.121 ... 0.229)	-0.37 (-0.78 ... -0.0056)	bad
NorESM1-M_rcp85_r1i1p1_REMO2015 (1)	good	reasonable	0.135 (0.0803 ... 0.172)	0.10 (-0.39 ... 0.78)	reasonable

5 Multi-method multi-model attribution

Table 5.1 shows Probability Ratios and change in intensity ΔI for models that passed model evaluation and also includes the values calculated from the fits with observations.

Table 5.1. Event magnitude, probability ratio and change in intensity for the 2024 observed Rx4day for observational datasets and corresponding estimates for 100-year return period for each model that passed the evaluation tests. (a) from pre-industrial climate to the present and (b) from the present to 2℃ above pre-industrial climate.

Observations / Model	2024 event /Threshold for return period 100 yr	(a) Pre-industrial (1.3C cooler) climate to present 2024 climate		(b) Present 2024 climate to future 2C warmer (than pre-industrial climate) world	
		Probability ratio PR [-]	Change in intensity ΔI [%]	Probability ratio PR [-]	Change in intensity ΔI [%]
ERA5 (1950-2024)	72.1 mm	4.6 (1.2 ... 54000)	18 (0.64 ... 36)		
EOBS(1950-2024)	50.7 mm	1.9 (0.20 ... 1600)	51 (45 ... 62)		
MSWEP (1979-2024)	63.8 mm	1.1 (0.0 ... 570)	-1.3 (-28 ... 36)		
E3SM-1-0 (1)	51 mm	2.4 (0.80 ... 8.6)	6.1 (-1.4 ... 15)	1.4 (1.1 ... 1.8)	2.4 (0.51 ... 4.2)
EC-Earth3-CC (1)	56 mm	2.0 (1.1 ... 5.1)	7.0 (0.62 ... 13)	1.6 (1.2 ... 2.1)	4.2 (1.9 ... 6.6)
EC-Earth3-Veg (1)	49 mm	1.2 (0.52 ... 5.0)	1.5 (-5.2 ... 9.0)	1.6 (1.2 ... 2.3)	3.6 (1.5 ... 5.5)
EC-Earth3-Veg-LR (1)	56 mm	1.9 (0.90 ... 6.6)	7.7 (-1.4 ... 19)	1.5 (1.2 ... 2.0)	4.1 (1.8 ... 6.8)
IPSL-CM6A-LR (1)	52 mm	1.6 (0.60 ... 6.4)	3.2 (-3.8 ... 11)	1.5 (1.2 ... 2.1)	3.3 (1.2 ... 5.4)
MPI-ESM1-2-HR (1)	58 mm	4.9 (0.86 ... 5.8e+2)	13 (-1.6 ... 29)	1.6 (1.2 ... 2.5)	4.2 (1.6 ... 7.0)
MPI-ESM1-2-LR (1)	52 mm	1.1 (0.43 ... 3.9)	1.1 (-7.5 ... 10)	1.1 (0.82 ... 1.7)	0.83 (-2.1 ... 4.2)
NESM3 (1)	56 mm	1.4 (0.37 ... 15)	2.4 (-7.0 ... 12)	1.4 (1.1 ... 2.1)	2.6 (0.43 ... 4.9)
CNRM-CM5_rcp85_r1i1p1_ETH-COSMO-crCLIM-v1-1 (1)	50 mm	25 (2.0 ... ∞)	19 (5.9 ... 36)	2.4 (1.5 ... 4.5)	5.4 (2.5 ... 8.5)
CNRM-CM5_rcp85_r1i1p1_RACMO22E (1)	45 mm	4.0 (0.072 ... ∞)	3.9 (-8.6 ... 19)	1.5 (0.29 ... 3.4)	1.5 (-2.2 ... 4.6)
CNRM-CM5_rcp85_r1i1p1_RegCM4-6 (1)	55 mm	1.6 (0.32 ... 25)	4.9 (-10 ... 21)	1.0 (0.71 ... 1.8)	0.34 (-4.0 ... 4.8)
CNRM-CM5_rcp85_r1i1p1_REMO2015 (1)	49 mm	11 (0.91 ... ∞)	15 (-0.85 ... 35)	1.6 (1.0 ... 2.8)	3.2 (0.17 ... 6.3)
CNRM-CM5_rcp85_r1i1p1_UGent-ALARO-0 (1)	51 mm	1.0 (0.30 ... 6.2)	0.25 (-8.9 ... 11)	1.2 (0.95 ... 2.2)	2.1 (-0.46 ... 5.4)
EC-EARTH_rcp85_r12i1p1_CCLM4-8-17 (1)	51 mm	21 (0.52 ... ∞)	14 (-5.7 ... 33)	2.2 (1.2 ... 4.6)	4.5 (1.1 ... 7.5)

EC-EARTH_rcp85_r12i1p1_ETH-COSMO-crCLIM-v1-1 (1)	51 mm	3.3 (0.89 ... ∞)	11 (-1.3 ... 27)	2.3 (1.6 ... 4.7)	6.9 (4.4 ... 9.5)
EC-EARTH_rcp85_r12i1p1_RegCM4-6 (1)	50 mm	3.4 (0.56 ... ∞)	10 (-5.6 ... 33)	2.2 (1.3 ... 5.2)	6.5 (2.6 ... 10)
EC-EARTH_rcp85_r3i1p1_RACMO22E (1)	54 mm	3.4 (0.50 ... 4.2e+3)	9.6 (-4.6 ... 24)	1.9 (1.2 ... 3.7)	5.7 (1.7 ... 9.6)
HadGEM2-ES_rcp85_r1i1p1_RACMO22E (1)	51 mm	21 (2.4 ... ∞)	16 (7.2 ... 29)	1.9 (1.3 ... 3.7)	5.7 (3.3 ... 8.1)
IPSL-CM5A-MR_rcp85_r1i1p1_RACMO22E (1)	56 mm	3.2 (0.80 ... 42)	9.8 (-1.7 ... 24)	2.0 (1.3 ... 3.0)	4.4 (1.2 ... 7.4)
IPSL-CM5A-MR_rcp85_r1i1p1_REMO2015 (1)	46 mm	1.6 (0.35 ... 87)	3.4 (-7.8 ... 17)	1.4 (0.86 ... 2.4)	2.0 (-1.0 ... 4.8)
MPI-ESM-LR_rcp85_r1i1p1_CCLM4-8-17 (1)	55 mm	1.9 (0.53 ... 15)	4.8 (-4.9 ... 16)	1.7 (1.1 ... 2.8)	4.6 (0.71 ... 8.0)
MPI-ESM-LR_rcp85_r1i1p1_ETH-COSMO-crCLIM-v1-1 (1)	55 mm	0.60 (0.22 ... 1.4)	-5.2 (-14 ... 3.4)	0.95 (0.62 ... 1.4)	-0.39 (-3.5 ... 2.6)
MPI-ESM-LR_rcp85_r1i1p1_RACMO22E (1)	47 mm	1.5 (0.17 ... 2.9e+2)	2.0 (-7.5 ... 13)	1.7 (1.0 ... 3.3)	3.6 (0.24 ... 6.5)
MPI-ESM-LR_rcp85_r1i1p1_RegCM4-6 (1)	52 mm	3.3 (0.61 ... 1.0e+3)	9.6 (-4.0 ... 27)	1.7 (1.2 ... 2.7)	4.9 (1.5 ... 7.9)
MPI-ESM-LR_rcp85_r1i1p1_WRF361H (1)	90 mm	1.2 (0.016 ... 17)	5.6 (-47 ... 69)	2.0 (1.2 ... 20)	11 (2.3 ... 17)
MPI-ESM-LR_rcp85_r2i1p1_CSC-REMO2009 (1)	49 mm	3.0 (0.95 ... 27)	8.9 (-0.28 ... 21)	1.5 (1.1 ... 2.3)	3.5 (0.49 ... 6.4)
MPI-ESM-LR_rcp85_r2i1p1_ETH-COSMO-crCLIM-v1-1 (1)	58 mm	2.1 (0.44 ... 19)	6.7 (-5.2 ... 19)	2.1 (1.4 ... 3.4)	6.0 (2.1 ... 9.5)
MPI-ESM-LR_rcp85_r3i1p1_REMO2015 (1)	46 mm	2.7 (0.96 ... 95)	7.9 (-0.30 ... 19)	1.7 (1.3 ... 2.8)	4.8 (2.3 ... 7.5)
NorESM1-M_rcp85_r1i1p1_ETH-COSMO-crCLIM-v1-1 (1)	54 mm	2.8 (0.90 ... 30)	12 (-1.1 ... 28)	1.3 (0.86 ... 2.7)	2.3 (-1.2 ... 5.8)
NorESM1-M_rcp85_r1i1p1_RACMO22E (1)	48 mm	1.2e+2 (3.0 ... ∞)	20 (9.0 ... 35)	2.1 (1.1 ... 5.6)	4.4 (0.47 ... 8.2)
NorESM1-M_rcp85_r1i1p1_REMO2015 (1)	44 mm	0.68 (0.11 ... 16)	-2.9 (-15 ... 15)	0.97 (0.55 ... 1.4)	-0.25 (-3.9 ... 3.2)

6 Hazard synthesis

The event studied in this analysis encompasses a very large region, and thus climatologically different subregions, some of which are mountainous while others are floodplains. Locally the rainfall that occurred from the large-scale Vb depression thus differed in intensity, duration and extent, not all of these are well represented in the observations. By analysing a four-day event over such a large region we therefore include different representations of these smaller scale processes which leads to discrepancies between the observations-based data products and thus comparably high uncertainty. All observations-based products show an increasing trend in annual RX4day in the study region since 1950 but differ in the strength. We note that observations are limited in places by quality issues in some of the observed data. This is also true when looking at observed trends in smaller regions, e.g. on a country scale (see section 3.1).

Given the impacts occurred over such a large region and the overall weather system causing the rainfall was equally large it is still informative to assess whether and to what extent human-induced climate change altered the likelihood and intensity of the 100-year return period RX4day rainfall in the area described above (section 1.2). To evaluate the influence of anthropogenic climate change on this defined event, we calculate the probability ratio as well as the change in intensity using observations and climate models. Models which do not pass the evaluation described above are excluded from the analysis. The aim is to synthesise results from models that pass the evaluation along with the observations-based products, to give an overarching attribution statement.

Figures 7 and 8 show the changes in probability and intensity for the observations (blue) and models (red) between the past and current , and current and future climates, respectively. The results are also shown in table 6.1. Before combining them into a synthesised assessment, first, a representation error is added (in quadrature) to the observations, to account for the difference between observations-based datasets that cannot be explained by natural variability. This is shown in these figures as white boxes around the light blue bars. The dark blue bar shows the average over the observation-based products. The combined results for the observations suggest a doubling in the likelihood of an event such as the one under study and an increase in intensity of about 20%, but with very large uncertainties including a decrease as well as an increase of more than a factor of 100 in likelihood and over 75% increase in intensity.

The dark red bar shows the model average, consisting of a weighted mean using the (uncorrelated) uncertainties due to natural variability. The uncertainty in the observational trend is large and encompasses the model results, however the model best estimate of an increase in likelihood by a factor of 1.69 and a change in intensity of 6.4% is much lower than the best estimate in observations. There are several possible reasons for this. For example, over such large scales, the precipitable water in the models is probably heavily constrained by a low moisture increase linked to the time of year being the (late) summer season. Also, the representation of the mountains in GCMs may be insufficient which may lead to the precipitation in the models being too weak, as well as an insufficient land-sea interaction. Furthermore, convection-permitting estimates have shown that increases in precipitation may have been underestimated in lower-resolution climate models (Kendon et al., 2020). Thus the rainfall in the models is underestimated which probably also means the trends are underestimated.

This means that when observation-based products and models are combined into a single result, the resulting attribution statement is likely also an underestimation. To combine the results, firstly, we

neglect common model uncertainties beyond the intermodel spread that is depicted by the model average, and compute the weighted average of models (dark red bar) and observations (dark blue bar): this is indicated by the magenta bar. As, due to common model uncertainties, model uncertainty can be larger than the intermodel spread, secondly, we also show the more conservative estimate of an unweighted, direct average of observations (dark red bar) and models (dark blue bar) contributing 50% each, indicated by the white box around the magenta bar in the synthesis figures. Due to the high uncertainty in the observations, the unweighted synthesis (white box) gives an unrealistically large uncertainty allowing for a strong decrease in heavy rainfall which for basic physics like the Clausius-Clayperon relationship we know is not correct for RX4day rainfall. We thus use the best estimates from the weighted synthesis, which gives a 7% increase in intensity and just under a doubling in likelihood as overarching results, but note that these are too conservative. We emphasise that the direction of change is very clear, but the rate is not.

The same caveats for the synthesised results given for the past-present comparison also hold when assessing the change in likelihood and intensity for both event definitions in a 0.7C warmer climate compared to today. Again we find that all models show an increase in likelihood and intensity, but it is relatively small with a factor of 1.5 and an increase in intensity of 4% for the best estimates. The latter in particular is comparably small compared to expectations from Clausius-Clapeyron and thus probably rather conservative.

While the analogue analysis described in section 1.1 does not indicate a change in the frequency of Vb systems, other drivers of the rainfall need to be studied, e.g. the role of the Mediterranean and Black seas surface temperatures, whether Vb weather systems and resulting cut-off lows move slower and thus bring more rain in one place, or if the water vapour content changes, to understand the full influence of human-induced climate change.

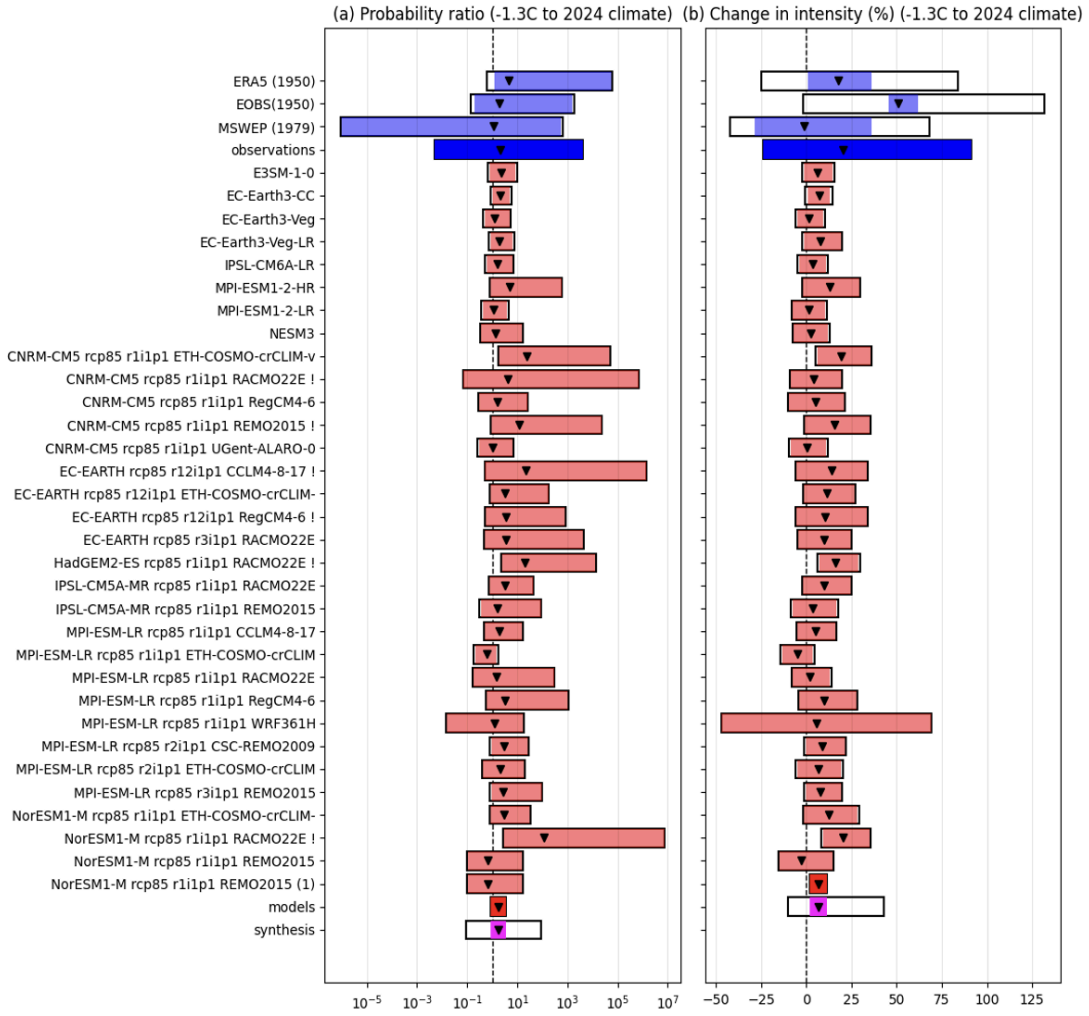

Figure 7. *Synthesis of intensity change (left) and probability ratios (right), when comparing the RX4day over the study region with a 1.3C cooler climate.*

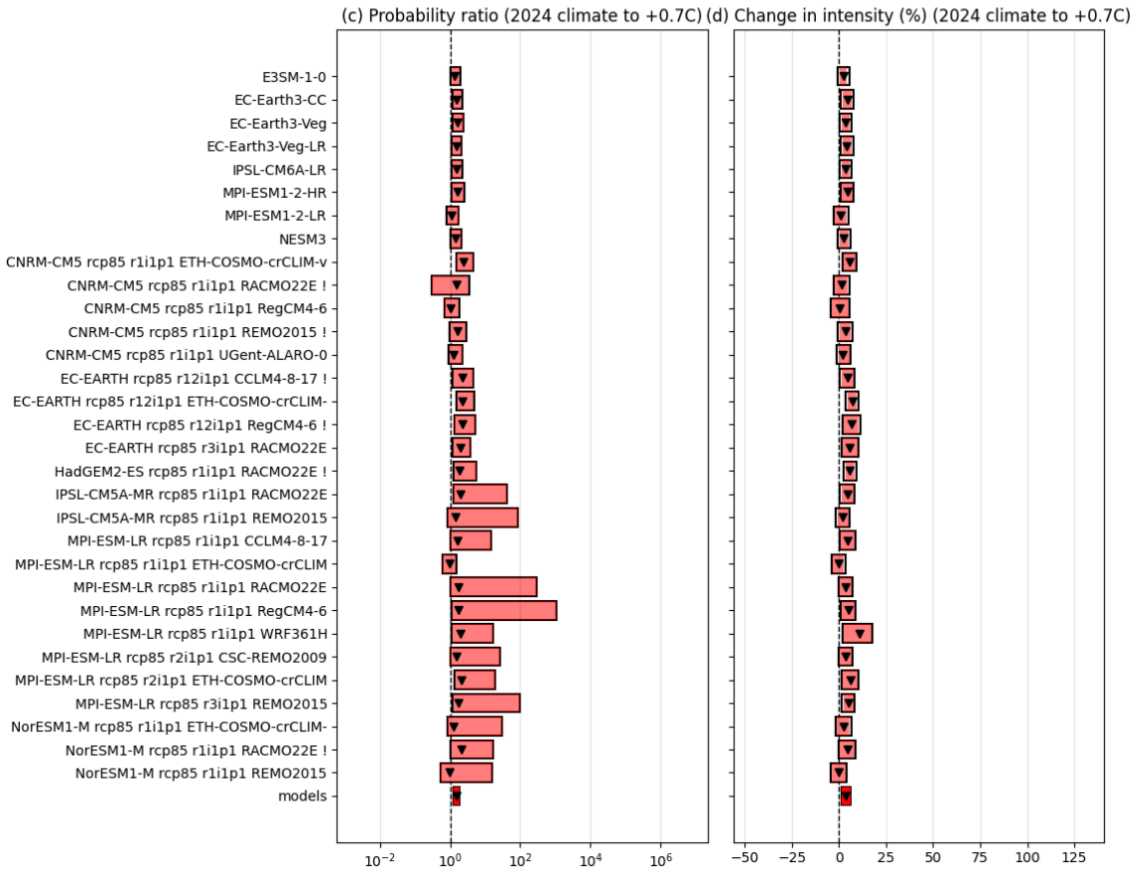

Figure 8. *Synthesis of intensity change (left) and probability ratios (right), when comparing the RX4day event over study region at 0.7°C warmer (2°C since pre-industrial) climate and the current climate for models*

Table 6.1: Summary of results for Rx4day, presented in Figs 7 and 8: Statistically significant increases in probability and intensity are highlighted in dark blue , while non-significant increases are highlighted in light blue .

Data	**GMST**		
		Probability ratio (95% CI)	**Intensity change (%) (95% CI)**
Observations	**Past- Present**	2.13 (0.00523 … 4170)	20.5 (-23.8 … 91.1)
Models		1.69 (0.872 … 3.48)	6.39 (1.84 … 11.2)
Synthesis		1.69 (0.878 … 3.48)	6.50 (1.97 … 11.3)
Models only	**Present- Future**	1.49 (1.22 … 1.84)	3.67 (1.33 … 6.06)

7 Vulnerability and exposure

The 2024 central and eastern European floods caused widespread devastation, affecting urban and rural populations across several countries. The floods are comparable to the floods in Germany, Czechia and Poland in 1997, which led to losses in excess of up to 8.3 billion US$ and at least 100 fatalities, and in 2002, when Germany, Austria and Czechia were hit by floods leading to 232 fatalities and a combined 20 billion US$ (Kundzewicz et al., 2013). The intensity and duration of the heavy rainfall over 13-15 September, exacerbated by climate change, tested, and in some cases overwhelmed, emergency response systems and local infrastructure. This vulnerability and exposure analysis examines the intersecting factors which contributed to or reduced the severity of the floods' impacts, with a particular focus on spatial planning, infrastructure, transboundary water management, flood protection, early warning systems, and emergency response. While further research and after action reviews will be necessary to complement this rapid analysis, it aims to offer insight for future flood risk management in the context of a continued changing climate.

7.1 Flood risk

In line with the EU Floods Directive (2007/60/EC), nations in the EU are mandated to create flood hazard and risk maps to assess flood risks (EUR-Lex, 2007). These maps display areas prone to flooding, water depths, and potential impacts under various flood scenarios, and are crucial for understanding and reducing flood risks by providing insights into areas that are most exposed. While Slovakia is yet to submit their second Flood Risk Management Plan to the Central Data Repository, Germany, Austria, Poland, Hungary, Slovenia, and Romania have done so), as per the second cycle (2016-2022), while now the third is underway (2022-2027) (European Commission, n.d.). The only non-EU Member State among the countries of focus in the study, Moldova faces economic and other resource constraints which hampers the country's work towards developing flood hazard and risk maps on a similarly granular level as required by the EU regulations.

Van Ginkel et al. (2021) conducted a continental-scale assessment of flood risk to the European road network, estimating an annual €230 million in direct damages from large river floods. Infrastructure along the transboundary Danube and Elbe rivers constitute particular hotspots. Similarly, a report by The World Bank (2021) assessing the financial risk of floods within the EU found that Germany is the most economically vulnerable to flooding due to its large economy and infrastructure. Suffering an estimated annual €7.9 billion due to riverine and flash floods, Germany is moreover expected to experience an 25% increase in average annual losses by 2050 (The World Bank, 2021). Similar losses in Poland, Czechia, Austria, Slovakia, Romania, and Hungary range between €333 million and €1.5 billion, with countries like Romania facing one of the highest proportional impacts, as their relative damage from flooding is more significant compared to their economic size (The World Bank, 2021).

The floods also resulted in damage to businesses and disruption of services, such as the shutdown of the Vienna train system, which in turn led to disruptions in business continuity and related economic impacts (Bloomberg, 2023).

7.2 Spatial planning and infrastructure

Floods have impacted numerous urban centers and critical infrastructure across Europe. Cities along major rivers are particularly vulnerable and exhibit a high exposure to floods (see figure 9) (Steinhause et al., 2022). The most severe urban impacts have occurred along the Polish-Czech border and in Austria (The Guardian, 2024). In Nysa, Poland, 44,000 residents, including hospital patients, were evacuated due to the risk of an embankment failure, and Wroclaw faces similar threats (BBC, 2024, Reuters, 2024). Ostrava, Czechia, experienced flooding in industrial areas, while over 70% of Litovel was submerged (Reuters, 2024, BBC, 2024). In Lower Austria and Vienna, 26 villages remain isolated and 1.750 people have been evacuated (Tagesschau, 2024, IFRC, 2024). Infrastructure damage has left 250,000 without power, and tens of thousands lack water and mobile networks across the region (Red Cross Climate Centre, 2024, Reuters, 2024, BBC, 2024, BNN News, 2024). As the situation continues to unfold, the full extent of the destruction remains unknown, and the figures are expected to change in the coming days and weeks. The data in this report reflects the available information from September 15 to 20, 2024.

Figure 9. *Map showing areas of potential significant flood risk across Europe. Source: Flood Risk Area Viewer (2024).*

Notably, areas currently affected had already been identified as high risk zones as vulnerability and risk assessments show for Wroclaw in Poland (Kundzewicz et al., 2023) affected regions in Austria (Leis and Kiefenberger, 2020), Bratislava in Slovakia (Vojtek, Janizadeh and Vojteková, 2022), the affected eastern regions Galati, Vaslu in Romania (Török et al., 2018) and Saxony, especially Dresden, in Germany (Steinhausen et al., 2022). A tenth of Europe's urban population is currently living in areas at risk of flooding (EEA, 2020). The reasons for the high degree of vulnerability and exposure, and hence risk, relate to a multitude of factors related to urban planning and land use. Dolejs et al. (2022) conducted an analysis of land use and land cover (LULC) across Germany, Austria, Czechia, Poland, and Slovakia, and found that urban sprawl and increasing built-up areas are driving an

increase in artificial surfaces (currently 15%) in flood plains.

Apart from preventing built up in flood plains and controlling urban sprawl, green and blue spaces, which can help absorb some of the excess water, are often insufficiently integrated into urban infrastructure and planning. Sodnik, Kogovšek and Mikoš (2015) highlight that the implementation of green spaces in countries like Slovenia or Czechia can be a challenge due to limited financial and personal resources compared to other European countries. In Czechia, out of 300 planned measures along the Odra river, only 19 were implemented and the general level of implementation to mitigate flood risk was assessed as very low (Kundzewicz et al., 2023). However, it's important to note that nature-based and green solutions are often unable to withstand the most extreme floods, and therefore, while they are important part of a flood adaptation plan, extreme floods like this one would require additional measures that reduce the exposure of people to flood risks (Esraz-Ul-Zannat et al., 2024). In fact, the combination of green and grey infrastructure is often more effective for flood mitigation than NbS alone (Esraz-Ul-Zannat et al., 2024). One study points to detention areas as the most cost-effective adaptation strategy to reduce peaks as a result of rising flood risks in Europe (Dottori, F., et al., 2022).

Yet some progress must be acknowledged. In Poland, 44 of the largest cities have developed adaptation plans, reaching up to 80% of the population (Ministry of Climate and Environment Poland, 2019). Wroclaw, Poland, has implemented a new drainage system, increased green spaces, built semi-permeable surface in parts of the city, and is planning to scale (UNDRR, 2022). Moreover, Ostrava, Czechia has published plans to improve rainwater runoffs, increase the proportion of permeable surfaces within the city, as well as regeneration of brownfields and post-industrial areas as green and blue spaces (Department of Strategic Development Ostrava, 2024).

7.3 Transboundary water governance, and flood protection

The recent floods in central and eastern Europe emphasize the need for coordinated water management strategies. Severe flooding occurred in rivers such as the Vltava and Opava in Czechia, and the Nysa in Poland, while major rivers like the Danube, Oder/Odra, Morava, and Elbe experienced significant water level rises (Cameron et al., 2024; Euro News, 2024). Shared by 19 countries, the Danube's floods caused dam failures and widespread disruptions in Austria, Slovakia, and Hungary, particularly affecting Bratislava, Budapest, and the Lower Austria region (see figure 10) which has been declared a disaster area (ICEYE, 2024; Henley, 2024; Easton et al., 2024). In Poland, the transboundary Oder/Odra River reached critical levels, threatening cities such as Ostrava, Bohumin, and Wroclaw (Euro News, 2024), while dam bursts in Lower Silesia resulted in fatalities and evacuations.

Figure 10. *Flood extent in Gänserndorf District, one of the hardest-hit districts in Lower Austria in the wider Vienna area, as of 18 September. Source: ICEYE, (2024).*

The Danube River Basin, the world's most international river, fosters extensive cooperation in flood management. The Danube River Protection Convention (1998) promotes sustainable water use and flood management but faces challenges, particularly in the eastern regions where maintenance is lacking (ICPDR, n.d.; Global Water Partnership, 2015). Similarly, the International Commission for the Protection of the Danube River (ICPDR) oversees flood risk management, supported by the Danube River Basin Flood Risk Management Plan, which enhances cross-border flood forecasting and communication (Pozo et al., 2015). For the Oder and Elbe rivers, the International Commissions for their protection coordinate joint flood management efforts (Federal Republic of Germany, 1992).

The catastrophic floods of 2002 along the Elbe and Danube caused widespread destruction of infrastructure, displacing thousands of people, and leading to substantial economic losses. The severity of these floods underscored the urgent need for a more robust and coordinated approach to flood preparedness, prompting the European Commission to create a pan-European flood early warning system. The Copernicus Emergency Management Service's European Flood Awareness System (EFAS) enhances flood monitoring and forecasting, providing information on upcoming floods to national and international forecasting and civil protection authorities including the European Commission's Emergency Response Coordination Centre (ERCC) (Copernicus, n.d.). EFAS particularly provides information to support flood forecasts for transnational rivers and provides information at longer lead times, helping to bridge gaps in national and international capability and improving preparedness across the continent (Pozo et al., 2015, Pappenberger et al. 2015). However, varying technical capabilities, discrepancies in national flood protection standards, and language barriers complicate coordinated responses. Efforts to address these issues include harmonizing flood risk assessments, joint flood protection projects, and international exercises to improve cross-border response (Pozo et al., 2015).

7.4 Forecasting and warning systems

In recent years there have been advances in both national capabilities in weather and flood warning, as well as in the underpinning weather and flood forecast modeling across Europe (Maybee, 2024; Mazzetti and Prudhomme, 2018; Najafi et al., 2024; ICPDR, 2023). The extreme rainfall and flooding from storm Boris was well-forecasted both by the European Flood Awareness System (EFAS) (red warning for Czechia and southern Poland and orange for much of central Europe) and by national meteorological services in central Europe days in advance of the first impacts (News.AZ, 2024, AP 2024; Climate Centre, 2024). One analysis estimates the benefits of the EFAS system are of the order of 400 Euro for every 1 Euro invested (Pappenberger et al., 2015). ARISTOTLE, the pilot European multi-hazard, transboundary early warning system was also activated, providing information to European Emergency Response Capacity (ERCC) days in advance of the floods (ARISTOTLE). Meteoalarm, the European early warning dissemination system also sent out warnings indicating the potential impacts of the floods, along with advice in the local language of each region (Meteoalarm). These are few examples amongst a network of flood monitoring, forecasting and warning systems that exist at continent, national and subnational scales in Europe.

Preventive measures based on forecasted rainfall were taken in some locations, for example along the Elbe in Dresden, Germany, as the river's levels rose (Henley, 2024). In Prague flood defenses were deployed including flood gates that were installed as part of 1 Billion Euro effort to prevent a repeat of the damages experienced in the 2022 floods (News.AZ, 2024). Across Czechia reservoirs were emptied in an attempt to accommodate the forecasted rainfall. Austria has also invested in flood management since the 2002 and 2013 floods, and in particular Vienna's flood defenses are designed to manage a 1-in-5,000 year flood, reportedly limiting the impacts in the city (BBC, 2024).

The number of fatalities reported from this flooding has reached 26, whereas in previous events in 1997 and 2002 114 and 232 people died, respectively. This shows the value of improvements to early warning systems and flood preparedness in the last two decades. However, any loss of life points to the need for significant improvements in land use planning, risk communication, emergency preparedness plans or flood defenses. News reports have highlighted that some of the victims of the September 2024 floods were elderly individuals (>70 years) who may have a harder time evacuating, pointing to the need to focus flood management efforts on the most vulnerable (Czech News Agency, 2024; Televiza Ta3, 2024).

7.5 Emergency response

Across the impacted countries, emergency responses were widespread, with national government declaring states of emergency, deploying military units, and mobilizing thousands of rescue personnel. Efforts to contain the crisis involved emergency funding, temporary mobile flood barriers, and evacuations. In Poland and Romania, among the worst-hit, thousands of people were evacuated, especially in the Oder, Vistula, Siret and Prut river basins. However, the destruction of infrastructure, including dams, bridges and roads, complicated rescue efforts.

Red Cross National Societies were involved in both preparedness and response activities alongside national and local authorities on the basis of their respective auxiliary roles. As the threat became clear, some assisted authorities in setting up flood protection measures such as sandbags, and providing support to those undertaking prevention activities. As the floods hit, the preparation turned to response, with some National Societies' directly involved in response planning and coordination with national and local authorities, taking part in emergency coordination meetings and sitting with their counterparts in emergency operations centres. Many mobilized their operational response leaders

and rapid response teams, and called in support from across their countries to the affected areas. While the activities of National Societies differed according to capacities, needs, and roles, they included: Evacuations and relocations, management or service provision of evacuation centres and temporary accommodation sites; provision of emergency medical services and First Aid; distribution of food, water, and essential household items; psychological first aid and support; provision of services for first responders; setting up domestic fundraising and item collection mechanisms; provision of dehumidifiers and drying equipment; and other activities. As the flood waters gradually subside and the extent of the damage becomes clearer, National Societies will continue to provide support to the return and recovery of affected populations.

V&E conclusions

The 2024 central European flood was well-forecasted and countries and cities knew about the potential for extreme floods days in advance, prompting some early actions that likely prevented impacts from becoming even more severe. However, infrastructure and emergency management systems built after lessons learned from previous floods have been severely tested and in many cases overwhelmed by the sheer magnitude and scale of this flood event, but climate models show that events like this (and worse) could become more frequent in future. Cities in flood-prone areas, already identified as hotspots, were hard-hit, with emergency responses struggling due to the scale of the disaster. While efforts to improve flood risk management are in place, gaps remain in areas such as integrating climate change into land use planning (EU, 2021). In a changing climate, this calls for stronger and better coordinated regional and national action on flood prevention and response.

Data availability

All time series used in the attribution analysis are available via the Climate Explorer. For data that is not, data is available upon request.

References

All references are given as hyperlinks in the text.

Appendix

Supplementary figures

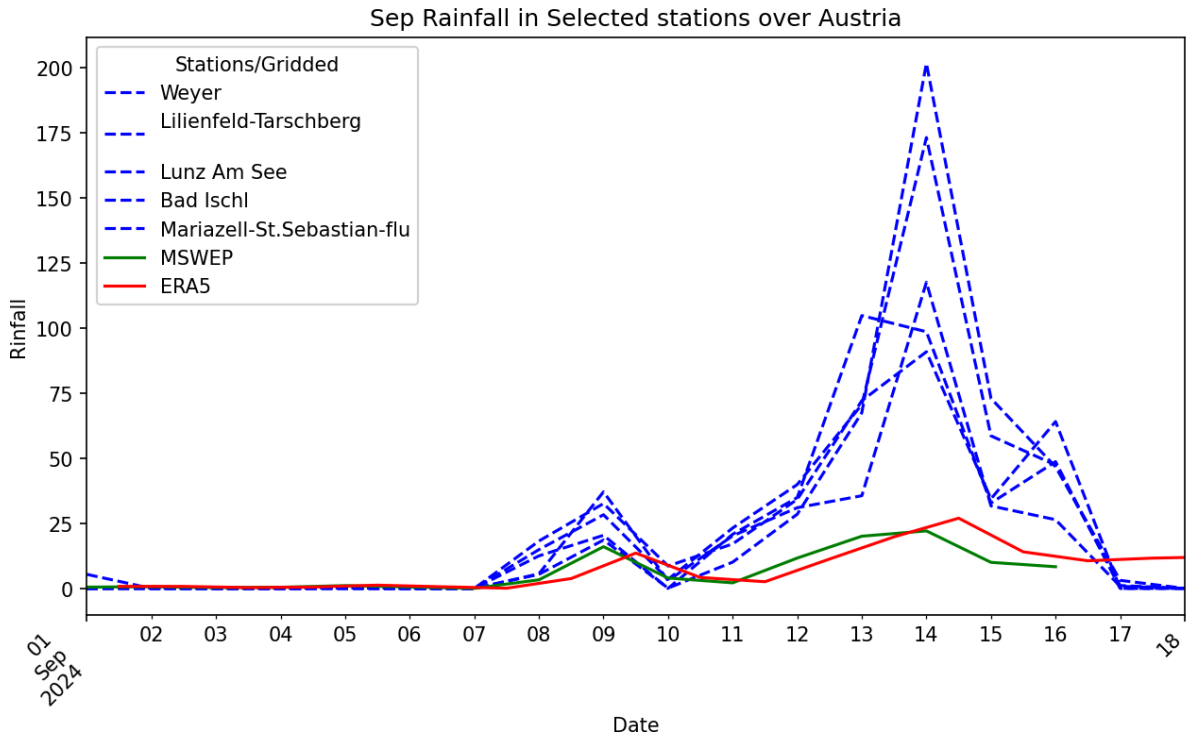

Figure S1: Daily evolution of rainfall in September 2024 in selected stations (blue dashed lines) over Austria vs. the gridded datasets- MSWEP and ERA5.

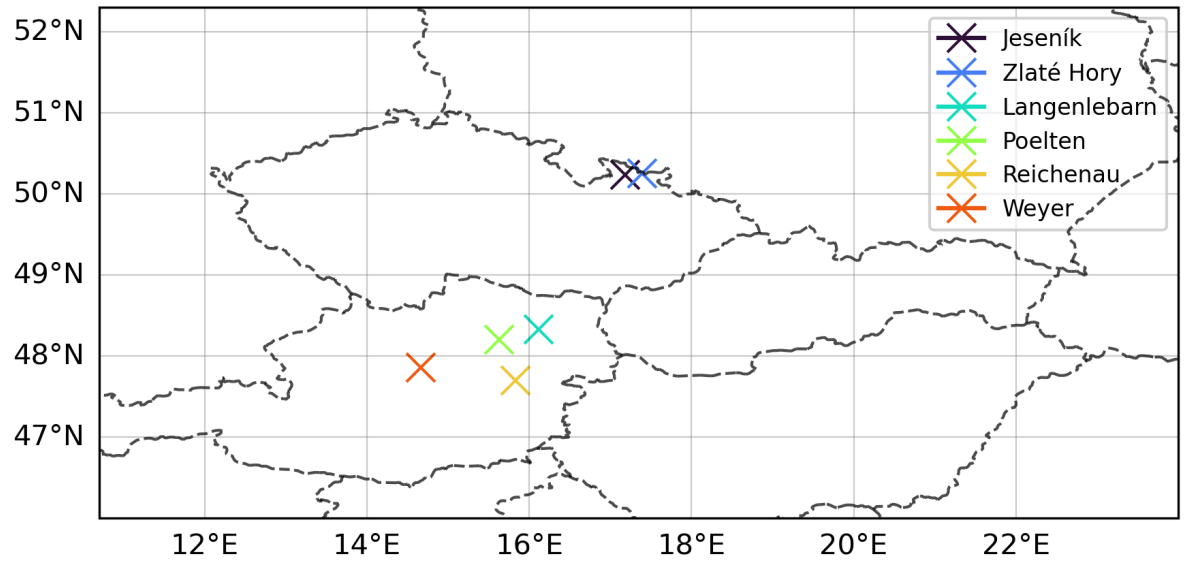

Figure S2: Location of local weather stations over the region that received the most intense precipitation from Storm Boris.

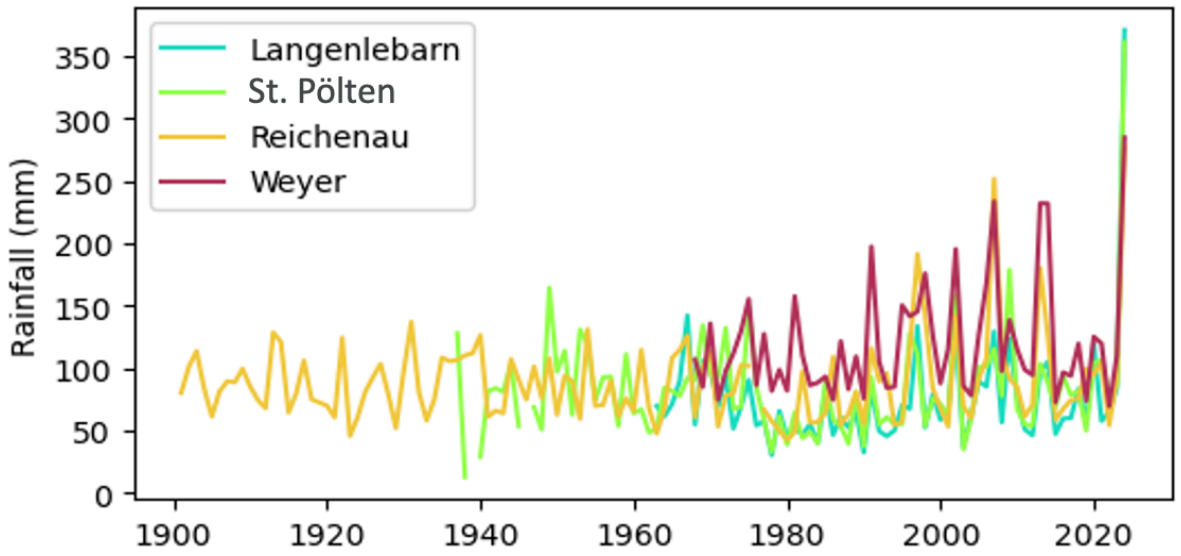

Figure S3: RX4day timeseries for selected stations in Austria (shown in figure S2) over the study region. The colours of the lines correspond to the stations in figure S2.

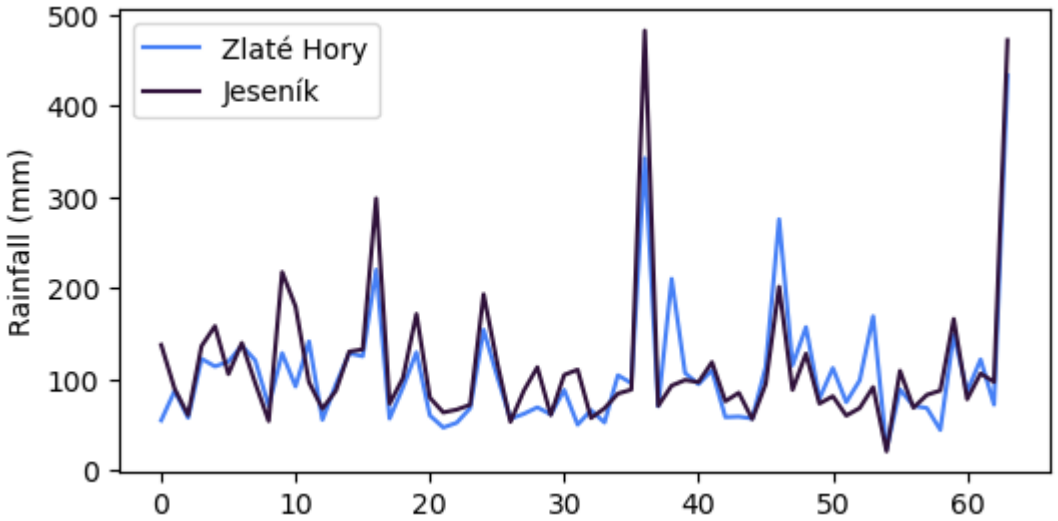

Figure S4: RX4day timeseries for selected stations in Czechia (shown in figure S2) over the study region. The colours of the lines correspond to the stations in figure S2.

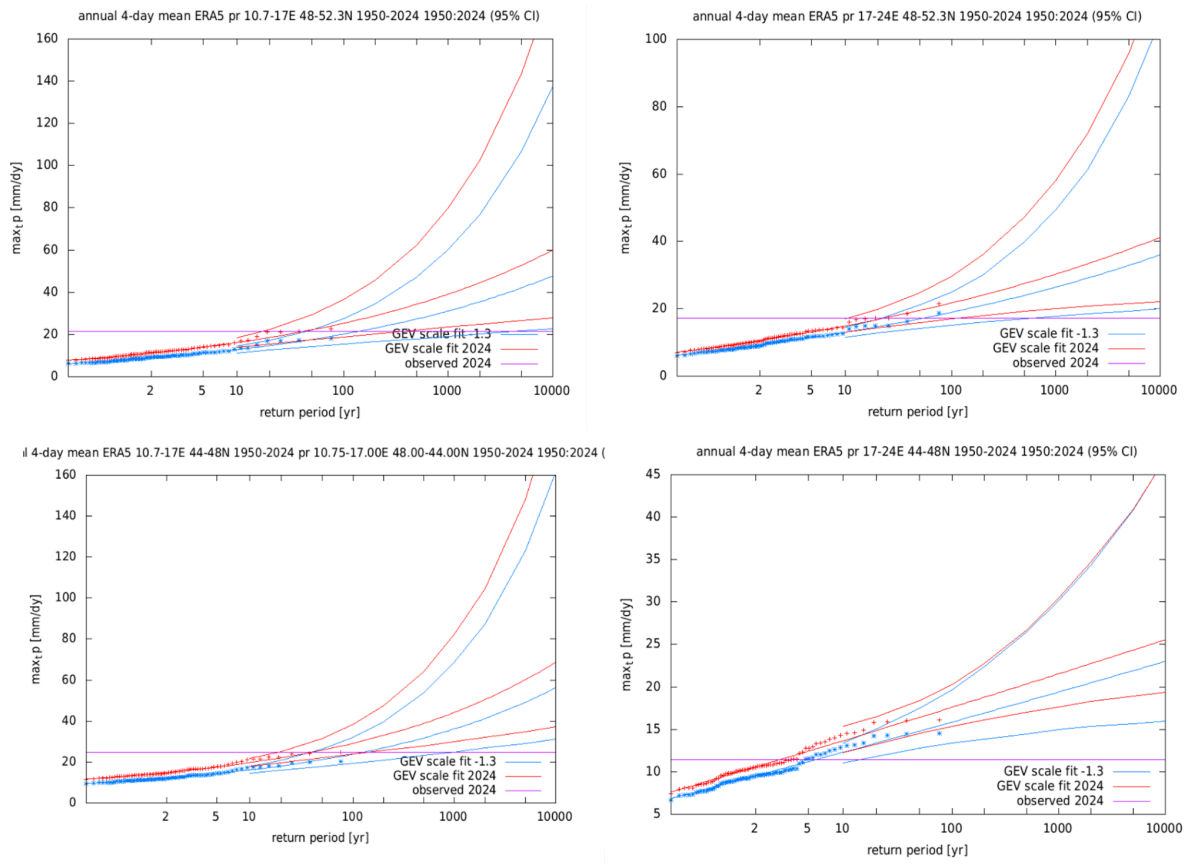

Figure S5: GEV fit to the RX4day timeseries for the four quadrants within the study region, displayed at present day and in a 1.3 C cooler world using the scale assumption. The plots are organised as follows - top left: Northwest, top right: Northeast, bottom left: Southwest, bottom right: Southeast.

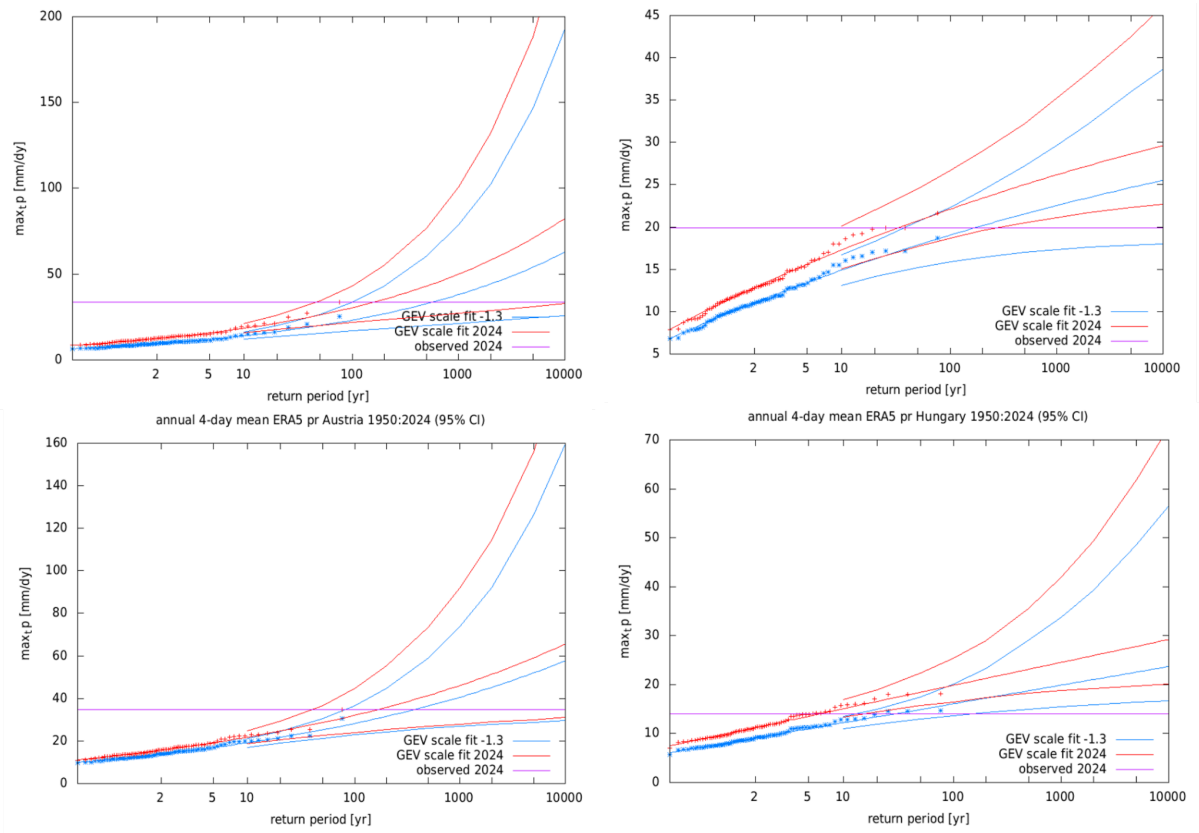

Figure S6: GEV fit to the RX4day timeseries for four nations within the study region, displayed at present day and in a 1.3 C cooler world using the scale assumption. The plots are organised as follows - top left: Czechia, top right: Slovakia, bottom left: Austria, bottom right: Hungary.